Title: ***Aerodynamics characteristics of butterfly flight through measurement of three-dimensional unsteady velocity field using TR-PIV system***

REF: AOARD-09-4102
Contract No. FA23860914102

PI: Debopam Das
Debopam Das; Ph. D.
Associate Professor
Department of Aerospace Engineering
Indian Institute of Technology Kanpur
Phone: +91 512 259 6163 /7227 /8578
Email: das@iitk.ac.in, Debopam_d@yahoo.com

Problem definition

The present work is divided into three major portions. One is the flow visualization, the other two being the force measurement and the PIV measurement. In the flow visualization carried out in water, the basic flow physics has been observed and later found to justify with the PIV results in the same Reynolds number range 5000-10000. In the force measurements the effect of parameters like wings size and flapping frequency is studied on various flapping models of different degrees of freedom. For the PIV measurements the wake profile, the vortex interactions and other flow features that takes place in such flapping flight are studied. Initially some suitable flapping models are chosen and the experiments of force measurements are carried out with and without forward velocity, whereas the PIV measurements and the flow visualizations are carried out at no forward velocity, thus shifting the level of study to completely unsteady regime (advance ratio<1). Finally the observations with the PIV analysis are compared with the force results to explain the nature of the forces and their patterns. Thus PIV experiments serve both as a tool of flow visualization as well as a quantitative judgment for studying the nature of flow over a flapping wing.

1. Introduction

Large lift generation capacity and efficient flying of natural flying objects has generated enormous amount of interest among scientists and engineers for decades. The intricate 3D unsteady motions of wings have made this study complex. However with the advancement of technology and improvements in experimental techniques the physics behind such flight can be much better understood than before. The application of uncovering the knowledge of physics of such flapping flight can be of significant interest while designing flying robots or MAVs (Micro Air vehicles) of flapping wing type. Though MAVs of fixed wing have been successfully made and implemented as it uses the same conventional aerodynamics of steady state, whereas flapping wing flight is still not clearly understood. The basic aerodynamics fails while accounting for the mechanisms or forces generated by flapping wing fliers as the existing theories are limited by the steady state hypothesis whereas the flapping flight is completely unsteady

Report Documentation Page

Form Approved
OMB No. 0704-0188

1. REPORT DATE	2. REPORT TYPE	3. DATES COVERED
24 JAN 2011	**FInal**	**01-08-2008 to 01-07-2010**

4. TITLE AND SUBTITLE	5a. CONTRACT NUMBER
Aerodynamics characteristics of butterfly flight through measurement of three-dimensional unsteady velocity field using TR-PIV system	5b. GRANT NUMBER
	5c. PROGRAM ELEMENT NUMBER
6. AUTHOR(S) **Debopam Das**	5d. PROJECT NUMBER
	5e. TASK NUMBER
	5f. WORK UNIT NUMBER
7. PERFORMING ORGANIZATION NAME(S) AND ADDRESS(ES) **Indian Institute of Technology Kanpur,IIT Kanpur,Kanpur,,Kanpur,,UP,208016**	8. PERFORMING ORGANIZATION REPORT NUMBER **N/A**
9. SPONSORING/MONITORING AGENCY NAME(S) AND ADDRESS(ES) **AOARD, UNIT 45002, APO, AP, 96337-5002**	10. SPONSOR/MONITOR'S ACRONYM(S) **AOARD**
	11. SPONSOR/MONITOR'S REPORT NUMBER(S) **AOARD-094102**

12. DISTRIBUTION/AVAILABILITY STATEMENT
Approved for public release; distribution unlimited

13. SUPPLEMENTARY NOTES

14. ABSTRACT
This report investigates understanding insect flight (having flapping and feathering motion) in view of lift & thrust generation, essential for flight control, with simultaneous measurement of velocity and forces. The present work is divided into two major portions. One being the flow visualization and PIV measurements, the other is force measurement.

15. SUBJECT TERMS
Fluid Dynamics, Aerodynamic Design and Analysis

16. SECURITY CLASSIFICATION OF:			17. LIMITATION OF ABSTRACT	18. NUMBER OF PAGES	19a. NAME OF RESPONSIBLE PERSON
a. REPORT **unclassified**	b. ABSTRACT **unclassified**	c. THIS PAGE **unclassified**	**Same as Report (SAR)**	**62**	

in nature and thus complicated three dimensional unsteady effects comes into picture and make the study complex.

Mechanisms responsible for unusually high generation of lift in the unsteady regime of consideration are discussed in this section. These mechanisms have been observed and studied but the replication of any of these into real scenario of MAVs have not been into much of progress yet. Still a lot of things are not fully understood. Even there exist several theories about the mechanisms and the subsequent lift generation which are mainly divided into the following.

Unsteady Leading Edge Vortex (LEV)

As air passes around the sharp leading edge of an insect wing, it breaks away from the wing and rolls up into a leading-edge vortex (LEV). LEV is a region of low pressure above the wing, and this provides an extra suction that increases the lift. LEVs are not new to aerodynamics, and indeed they keep delta-winged aircraft like Concorde and many other Fighter jet planes up in the air, where the LEVs are generated passively by the swept leading edge of the wing. What is unexpected and amazing about insect flight is that the LEVs are created and stabilised by the flapping motion itself. What would have been expected is as the LEV forms, the flow should continue to feed into the LEV. This would normally cause the vortex to grow so large that it breaks away from the wing, normalizing the low pressure zone, ruining the lift, and stalling the wing. However, it has been discovered that the flapping motion causes the LEV to spiral out to the wingtip, siphoning off the vortex and delaying the stall. The augmented lift, coupled with the delayed stall, is the principle mechanism that insects use for generating lift. It has been shown in this study as well, that this LEV stays in the total downstroke and even in some part of the upstroke when it should have been dispersed and dissolved. LEV accounts for 60-70% of the total lift generated as reported earlier in the literature.

The reasons of this delayed stall and stabilization of this LEV is explained by many theories. Three distinct categories of insect LEV structure have been described on the basis of studies with real insects and mechanical flapping models (Rayner, 1979). These three categories of LEV are summarized in Fig.1. The differences between these flow-fields are non-trivial. The three categories of LEV have qualitatively different flow topologies, corresponding to qualitatively different local solutions to the Navier–Stokes equations (Thomas et al., 2004). Moreover, because the topology of the vortex differs qualitatively between the three categories of LEV structure, the overall size of the vortex and its contribution to the total lift generated by the model/insect can only be calculated correctly if the correct topology is used.

ROTATIONAL LIFT

When an insect reaches the end of the upstroke, it must rotate its wings to place them at the correct angle of attack for the start of the downstroke. Similarly, the wings must flip over between the downstroke and upstroke. This is to take advantage of the interaction among the various vertical structures developed over and below the wing and enhance or

delay any shedding. Ellington first suggested in 1984 that these rapid rotations could produce extra lift, drawing on some experimental and theoretical results for aeroplane wings with rapidly increasing angles of attack. Michael Dickinson's group, working at Berkeley with a mechanical model of a fruit fly, clearly demonstrated this effect in 1999. Not only is this lift important for weight support, but it is also a potent mechanism for flight control. Dickinson speculates that fruit flies generate steering torques by carefully adjusting the timing of wing rotation at the stroke transitions. The same has been observed in the present study even later discussed.

WAKE CAPTURE

Insects generate lift and thrust by producing and shedding vortices from their wings. These vortices move with the wake as spiralling masses of air that slowly decay and disappear, rather like the tip vortices of aeroplanes. For insects with high wingbeat frequencies, such as flies, the vortices move only a short distance before the wing returns in the cycle, and they can use this as a point of leverage for generating additional lift.

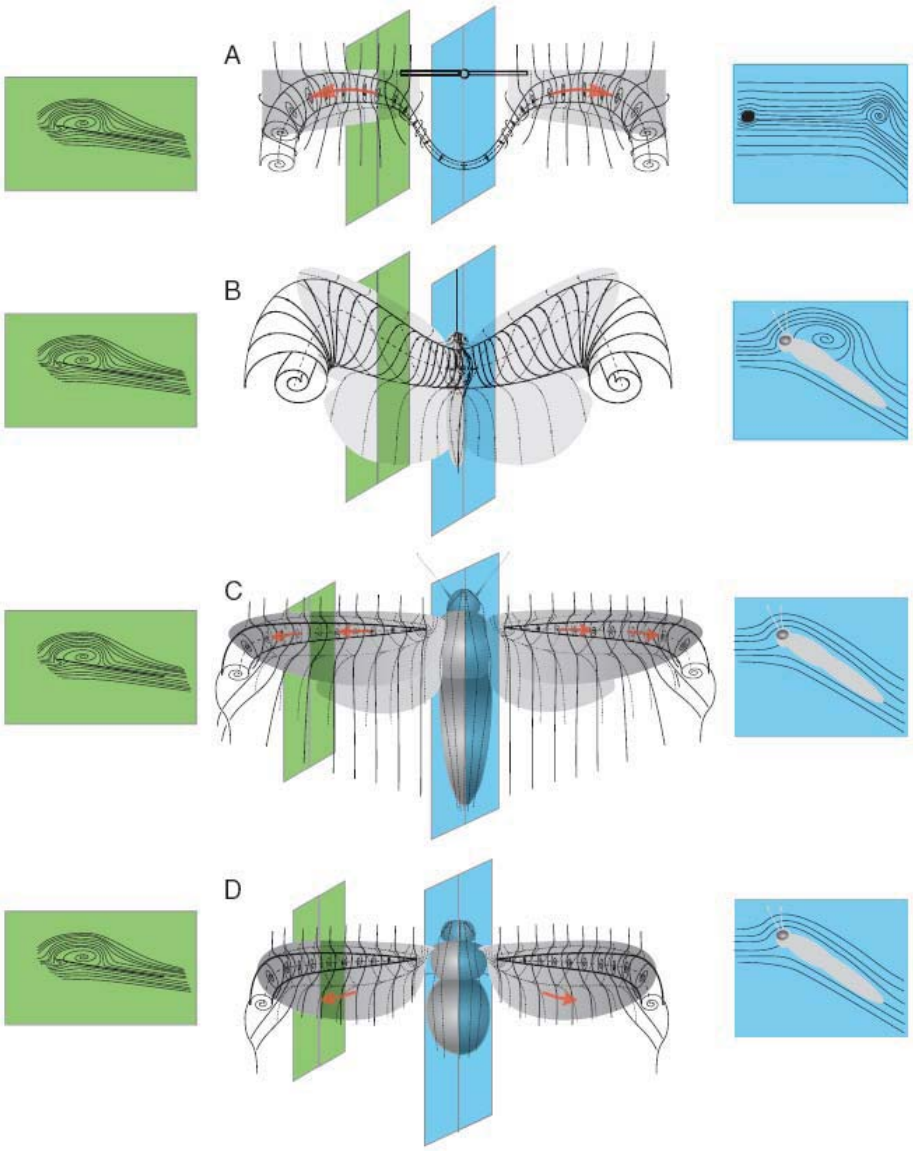

Figure1.1 (taken from R J Bomphrey et al, 2004) (A) Class I: The LEV inflects into tip and root vortices on each wing. The tip vortices connect to form a vortex ring behind the model, and the root vortices also connect so that the wake consists of one continuous vortex loop of complex shape. (B) Class II: LEV extending across the thorax of a hawkmoth and inflecting to form both tip vortices. There is no significant spanwise flow. (C) Class III: the structure described by Ellington and colleagues (Ellington et al., 1996; Van den Berg and Ellington, 1997a). In this model there must be a surface-bound focus at the base of each wing and attached flow over the thorax. (D) Also Class III: the flow, topologically similar to C, scaled for *Drosophila* by Birch and Dickinson (2001).

This process of ‘wake capture’, described by Dickinson's group in 1999, is another mechanism that fruit flies use for generating extra lift. This mechanism, unlike the LEV, might not be a widespread phenomenon because it needs a relatively high wing beat frequency. But it does suggest that other mechanisms whereby vortices interact might be useful for generating lift or torques for steering. Apart from this these shed vortices are high energy containing structures which are utilized back again in the subsequent stroke as the wing comes back before these vortices could move along with the wake. This saves power and enhances the flapping efficiency. The disturbance and unsteadiness the wing generates, it passes over the same again and again saving the effort required and produces some lift and thrust as well. Current research is investigating insects with two pairs of wings (forewings and hindwings) such as locusts and dragonflies. The forewings produce and shed vortices and their interaction with the flapping hindwings and the vortices that they are creating is not yet understood.

CLAP AND FLING

This mechanism has been extensively been studied by Weis-Fogh (1973). As the terminology suggests, it advantageously makes use of the interaction between two wings as they near each other at the extreme ends of the stroke, providing that the total flapping angle is nearly 180^{o}. Fig 1.2 depicts the wing kinematics and the consequent vortex development for a clap and fling motion.

The wing surfaces press together at the end of the upstroke for an extended period of time, mimicking a motion much like two hands coming together for a clap. As the wings separate and open for the next downstroke, they rotate around their trailing edges. The trailing edges remain adjacent and connected together until the included angle reaches 120^{o}. At this instant, the wings form a V-shape before they begin parting away from each other. The sudden translation of opposing section causes air to rush into the widening gap and produce high strength vortices of equal and opposite sign. This leads to a large circulation and lift in the wing without the negatives of vortex shedding since the total circulation around both wings remains zero. Significant amount of work has been done by people over this clap and fling mechanism and the fluid dynamics underneath it. Again this clap and fling helps in the sustaining of lift in the upstroke by vortex ejections twice at the start and end of the clap mechanism. In this study also the same is being used in the experimental model.

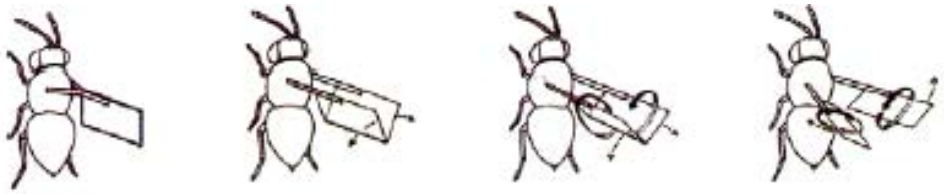

Figure 1.2 Clap and fling mechanism for housefly (Ref. C P Ellington, 1999)

Overview

The aim of the experiments conducted is to understand the nature of flapping flight through measurements of velocity field and aerodynamic forces generated in the flapping process. The forces generated are reasoned and justified through the visualization of flowfield and PIV results. The growth of LEV is intended to be studied. Thus the PIV experiments are to be performed at different chord sections of each wing to find out the class of LEV involved in this particular case. Again the difference across the different sections of a wing is observed and repeatability is checked out to be sure of the results. The same process is repeated for other wings as well so as to figure out any difference in the flowfield or timing of any significant mechanism with the change in wing size or the flapping frequency. For the force measurement, once the model is set up in the wind tunne with load cell, only wing change, wind veloity change and frequency variation are required for force study. Whereas for PIV measurements a partially closed container of glass or any other transparent material on 2sides is used to check the amount of smoke around the wing nearly same every time lending the control over the seeding particle density which has to be maintained at an uniform level for getting good data. Again for the general understanding of the nature of flowfield some visualization experiments are conducted in water to check the dependency on the flowfield on the same Reynolds number range.

Models

For our experiments of force and PIV measurements three different models have been used. Proper study of the flow properties and the flow field as a whole will not be appropriate until the models are well made with different degrees of freedom with the close simulation of the real case or near resemblance to natural fliers. Here the model resemblance is with the monarch butterflies thus the flapping angle, time of flapping cycle, range of flapping frequencies and size of the wing are made close to the real monarch butterfly. Though there are many forms and types of butterfly found in nature varying in types and shapes and flying parameters, monarch is chosen which uses a clap and fling mechanism with total flapping angle around 90^0. The same has been incorporated in one of the model as such. Wing is made of Mylar membrane which is scaled as per the wing of an average monarch butterfly (Fig1.3). Then two more scaled sizes are made to account for the variation in lift and thrust with wing size. Two other models have been chosen to study the effects of feathering and lagging in addition to flapping.

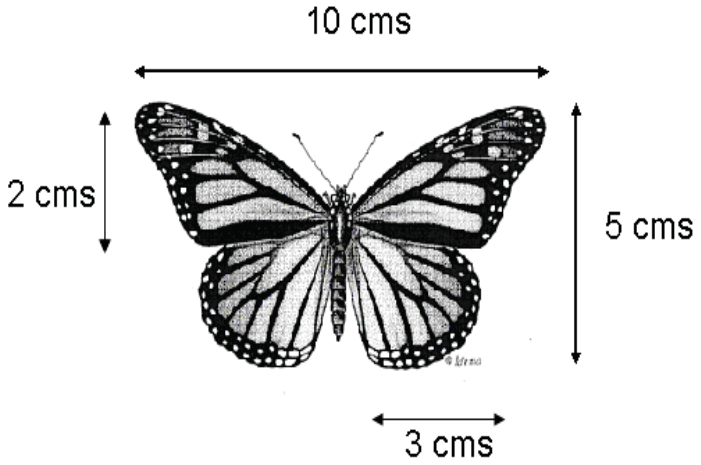

Figure 1.3 1X model of the monarch butterfly wing with dimensions.

Model 1

The first model simulates flapping motion with a 4 bar quick-return mechanism as shown in Fig 1.4. It has only one degree of freedom of flapping with time difference in the two strokes (downstroke and upstroke) of the flapping cycle. The time ratio is 1.3 where downstroke is slower. The reason to choose a flapping mechanism with a relatively larger downstroke time is chosen based on the observed flight patterns of flying animals with advance ratio J <1 such as bats and certain insects. Usually the maximum time ratio is 1:2 and it varies with the speed of flight and hence species (Hendrick et al, 2002 and Tobalske et al, 2003). The wing leading edge is glued to the flapping linkage arm with which it flaps as shown in Fig 1.4. The free end of the wing deflects a little during flapping motion adding to the feathering effect. The bigger the wing the more feathering it undergoes. For the wings we have considered the feathering angle that comes into play is less. But a little change in feathering angle also changes the dynamics of the force generation considerably. The insect model wing is a scaled model of monarch butterfly with a 1X (corresponds to the original size shown in Fig 1.3.), 1.5X and 1.75X (1.5 and 1.75 times of 1X model in span and chord wise directions). Force measurements are carried out for all three wings and PIV experiments are performed with the largest and smallest wing. Apart from the butterfly shaped wings, 3 rectangular wings of various aspect ratios of span length of 9cms are used for the force measurements while experimenting in wind tunnel.

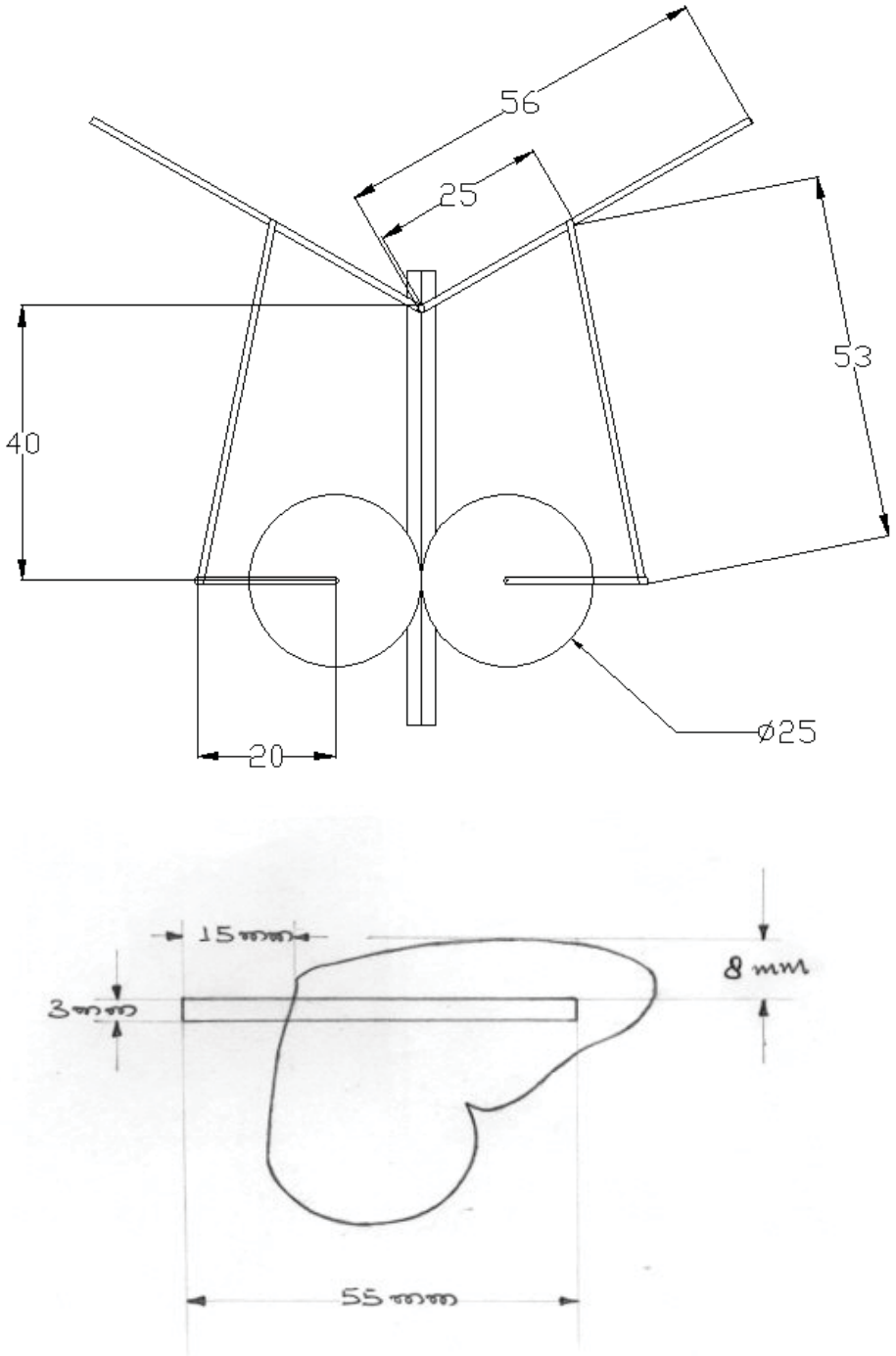

Figure 1.4 Schematic view of model 1 and wing mounting (all units in mm)

Model 2

The effect of flapping (clap and fling) motion has been incorporated in the model 1. In the model 2, effect of feathering is incorporated in the mechanism and the wing undergoes both flapping and feathering by the linkage mechanism itself (see Fig.1.5). Here the wing is fixed in a frame and thus there is no feathering effect due to deflection. The feathering effects are obtained by the mechanism alone. The model 2 is made with less angle of flapping so as to study the effect of the net angle of flapping if any on the flowfield. Due to structural changes and requirement of a high torque motor to overcome the resistance in the feathering part of the mechanism, the model is bigger and heavier. Hence force measurements are not done with this model due to the constraints of the load cell. Only PIV experiments are carried out with this model.

Model 3

Apart from flapping and feathering, lagging motion is also incorporated in this model (Fig 1.6). This is a miniature model, the force experiments are performed with this model. Here, even the same wings are used as done with model 1. But due to feathering and lagging motion the net swept angle of flapping became very large. The force estimation is done with load cells, so as to make out whether the lagging effect is making any change in the forces generated. PIV experiments have also been carried out on this model. PIV experiments are also carried out at 0.5R of the 1.75X wing mounted on it.

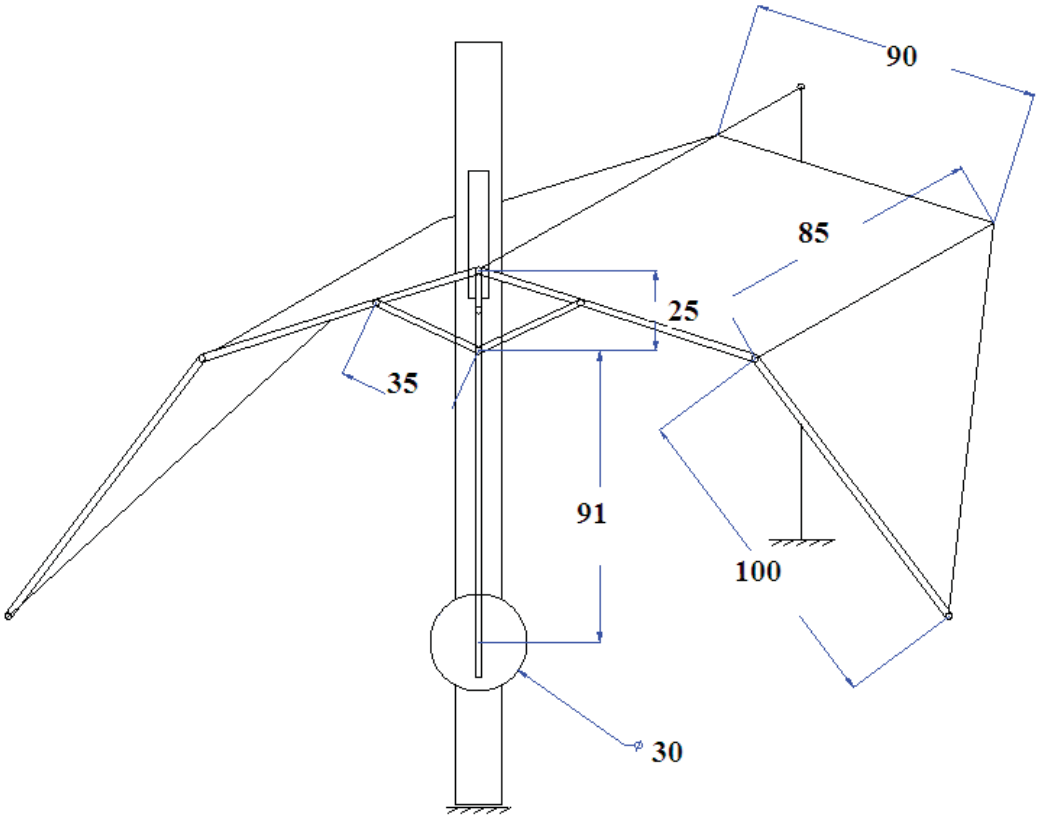

Figure 1.5 Schematic diagram of model 2 (all units are in mm)

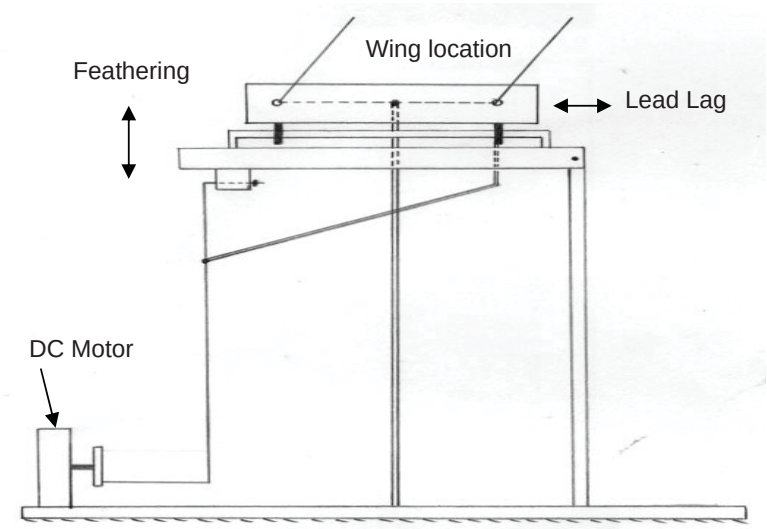

Figure 1.6 schematic view of model 3

2. Flow visualization

To understand the complex unsteady mechanism of unusually high force generation through flapping wing, flow visualization experiments were carried out. Flow features of such unsteady flow are usually complex and dominated with vortical structures. Efforts have been made to visualize such vortex dominated flow and understand its role in flapping flight.

2.1 Experimental setup

Extensive visualization experiments were carried out to understand the complex unsteady flow structures during flapping motion. Periodic clap and fling motion of the wing is associated with vortex formation around the entire wing edge and ejection of vortex rings The aim of the flow visualization here is to provide more insights towards understanding the role of vortices in generating aerodynamic lift and thrust.

All the visualization experiments were conducted in a water tank made of 6mm glass and Perspex sheets. A light sheet was used to illuminate a particular plane of the flow field in study. A video camera (SONY DCR-VX2100E PAL) (25 frames/s) is mounted on top of the setup in such a way that it is perpendicular to the light sheet and captures the entire phenomenon in that plane. The schematic sketch is shown in Figs 2.1 and 2.2. The flapping wing mechanism is placed on the tank in such a way that the wing is completely immersed in water, even at the end stroke position.

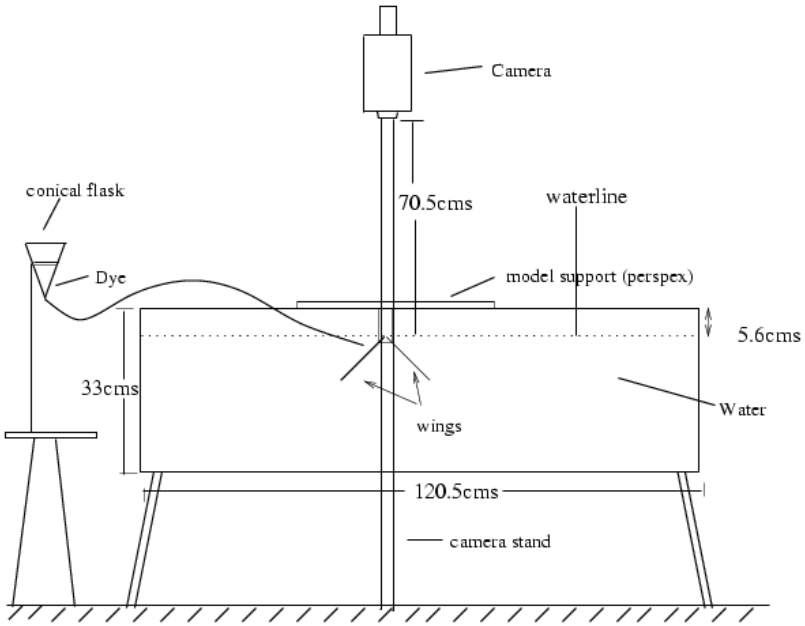

Fig 2.1 Diagrammatic representation of the flow visualization setup (front view)

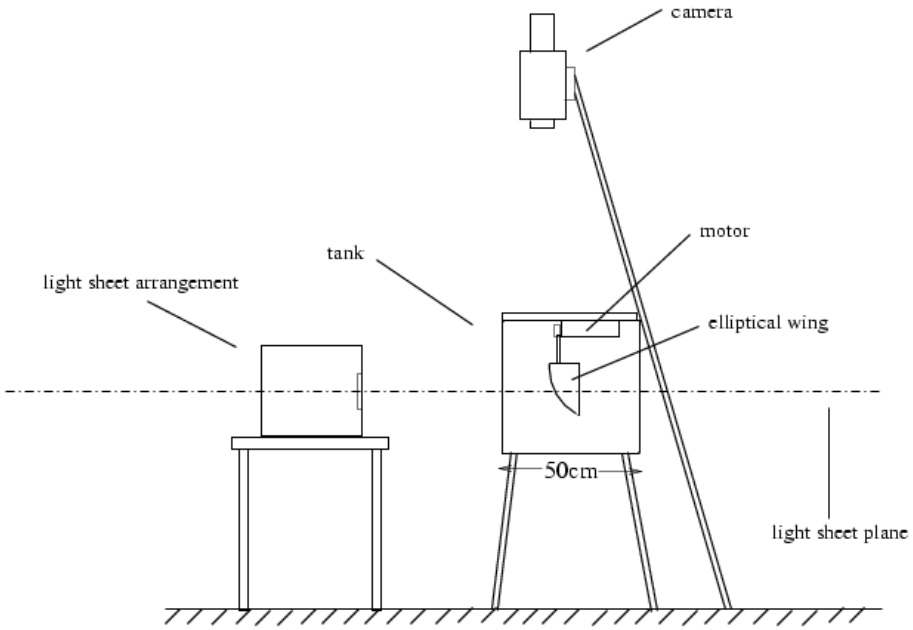

Fig 2.2 Diagrammatic representation of the flow visualization setup (side view)

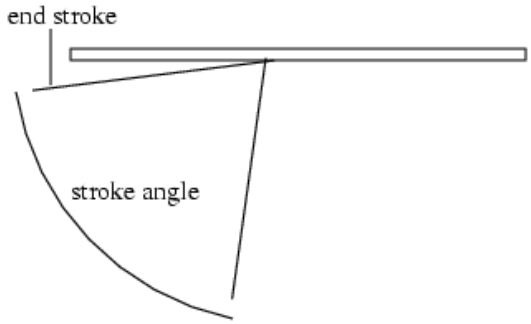

Fig 2.3 Stroke angle of the wing (front view)

The frequency of flapping at which experiments were performed is 0.46Hz and 0.7Hz for single wing model and 0.2Hz for double wing model. The models were placed upside down such that the motor can be kept outside the water level. A light sheet was used to illuminate a particular plane and flow field was visualized using a camera perpendicular to this plane.

Experiments have been carried out in a water tank, with size (150cmsX50cmsX75cms). The experimental arrangement is shown in Fig 2.1-2.2. Fluorescent dye has been used for tracing the fluid path. Dye was injected before the start of the flapping on the wing in suitable positions.

Shape and size of single wing model used for flow visualization is shown in Fig 2.4. The flapping frequency of the model is 0.46 Hz. The total angle of flapping for this wing is 60^0 and the wing is started from a position 10^0 away from complete clap. The

visualization sequence given above shows some critical features during transition from upstroke to downstroke and vice-versa.

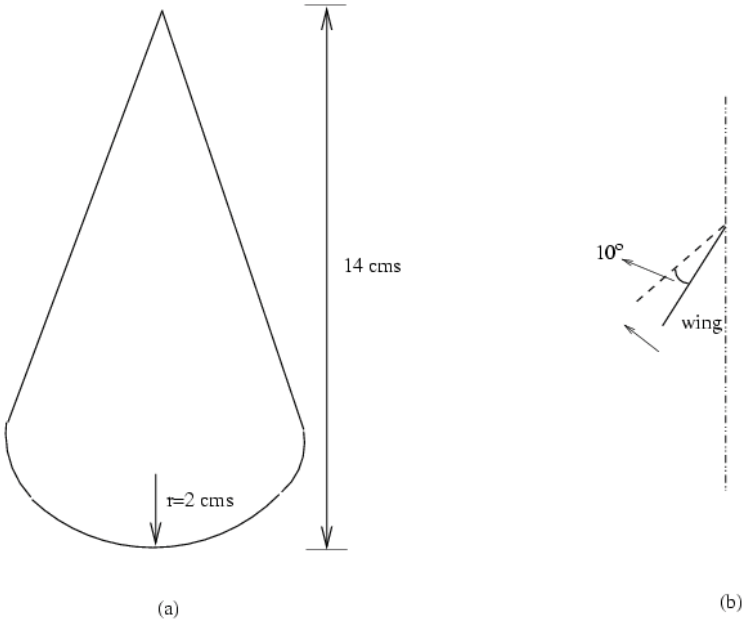

Fig 2.4(a) Dimensions of the symmetrical wing (b) wing at the starting position

2.2 Results

In Fig 2.5 (a), the motion has just started towards left (marked as face A). A vortex, say (V_1) has rolled up on the leading edge of face B as expected. The vortex has grown with time as can be seen in the subsequent pictures (Fig 2.5(b)-(d)). In Fig 2.5(d), wing has just started moving towards right. As soon as the wing starts moving in an opposite direction, a small vortex is formed on the face A of the wing. Interaction of this vortex V_2 with the vortex V_1 forms a mushroom shaped vortex pair Fig 2.5(f) which is then ejected at an angle. These two vortices (LEV pair) are formed during the start of the downstroke. The interaction between these two vortex rings formed around the wing, and its movement in an angular direction w.r.t. the wing is mainly responsible for the unusually high lift generated by insects (butterflies). We have observed similar structures during the fling-motion for a double wing, when the total angle of the fling is approximately 60^0. In (g) we can see a residual vortex remains on face B of the wing, which rolls over to face A of the wing in subsequent motion. In (i), breakdown of the vortex structure which was been ejected has been observed. However, a portion of initial vortex has rolled over to the other side of the wing (Fig 2.5 (h), (i)) and is being dragged along in the downstroke motion. Since the wing is re-utilizing this vortex (as it was created in an earlier stroke), this phenomenon is known as '*Wake Capture*'. The vortex is known as the stopping vortex. Wake capture increases the size of the stopping vortex as seen in (i), (j) and (k). In (o), the wing has started return the stroke after completing the stroke described from (d)-(n). Vortex is again being ejected at some angle during the return.

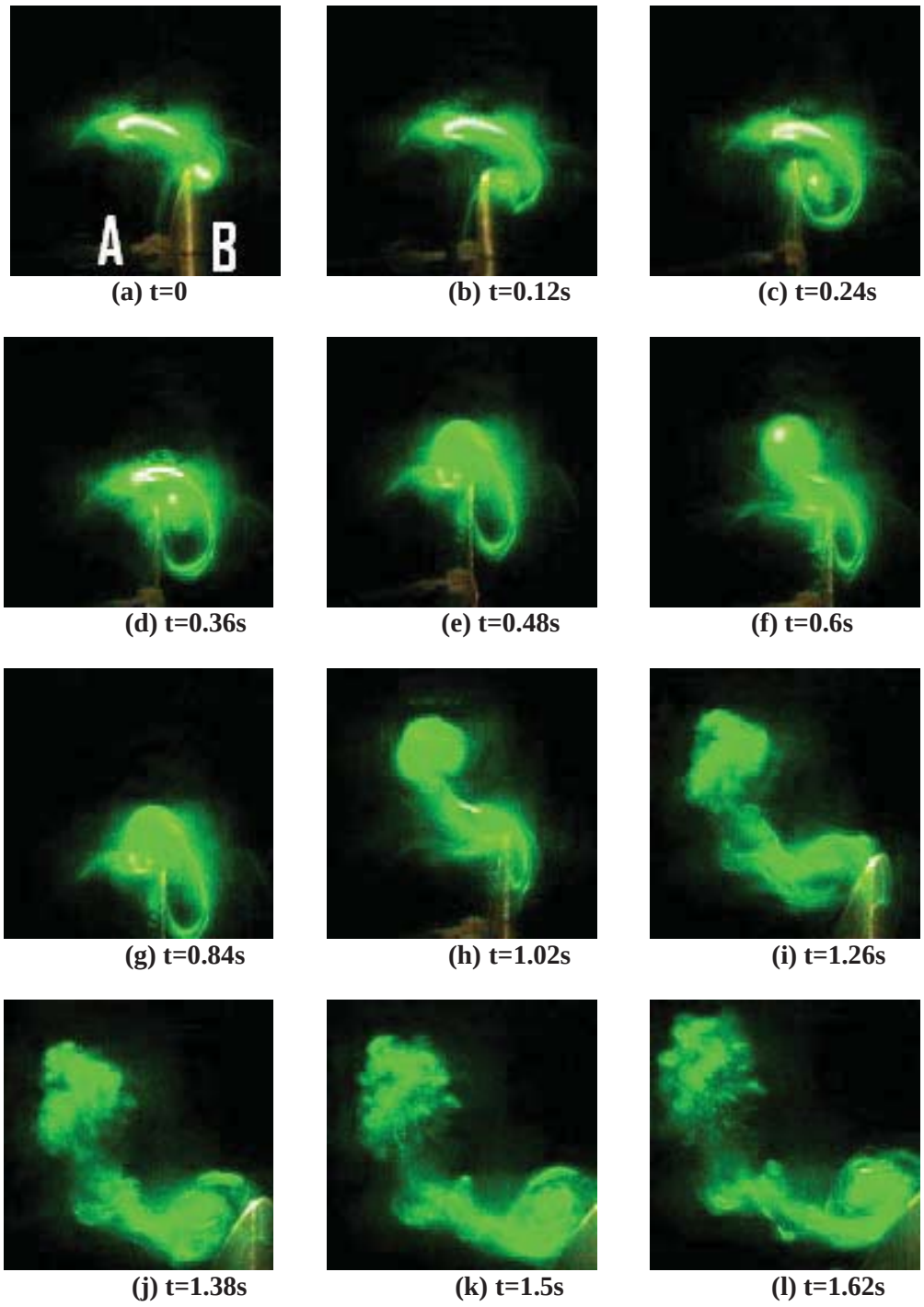

(a) t=0 **(b) t=0.12s** **(c) t=0.24s**

(d) t=0.36s **(e) t=0.48s** **(f) t=0.6s**

(g) t=0.84s **(h) t=1.02s** **(i) t=1.26s**

(j) t=1.38s **(k) t=1.5s** **(l) t=1.62s**

Fig 2.5 Vortex shedding visualization series (f=0.46Hz, symmetric single wing, span=14cms)

(m) t=1.74s **(n) t=1.86s** **(o) t=1.98s**

Fig 2.5 Vortex shedding visualization series (f=0.46Hz, symmetric single wing, span=14cms)

2.3 Conclusions

The leading edge vortex and its growth along the downstroke are observed. The phenomena of wake capture and ejection due to vortex interactions are also observed. The same has been again verified by the PIV results in the later section. Thus the vortex dominated flow features are a common phenomena for flappingwing type flight provided they are in the same Re range and the timing and levels of interaction and behaviour of these vortex pairs do depend on the wing material and its flexibility.

3. Force measurement

Earlier the force measurements are carried out by placing the model over a two component platform balance. Load cells are connected to a signal conditioner (Fig2.6) which is finally connected to the computer using the NI 4472 card. A lab view interface program is used for acquisition of the signals. The program mainly acquires voltage readings from the load cell which is calibrated to forces using known weights.
Measurements are performed in the wind tunnel with and without forward velocities using a new load cell (ATI 2kgs maximum load). With this new load cell the model 1 and model 3 are only tested.

3.1 Force results

At J=0

The data from load cell experiments are in terms of voltage and contained significant higher frequency noise at low flapping frequencies. The noise is eliminated using filters. Voltage data is converted to force using appropriate calibration of load cell. To remove the higher frequency noise a low pass filter is used in Matlab to filter out any frequency over 25 Hz. The flapping frequency is calculated by taking the FFT (fast Fourier transform) of this filtered data which is seen as a major peak in the plot (Fig 3.1d). This frequency is cross checked by the visualization using PIV. Fig 3.1 shows the processing of the data in steps. Fig 3.1a shows the raw data for 1X wing when supplied with 8V to the dc motor (Flapping frequency = 12.3Hz). After filtering the noise (> 25 Hz) the data is Shown in Fig 3.1b. After shifting the scale to zero and multiplying with the calibration coefficient the data is shown in Fig 3.1c. An enlarged view of the same can be seen in Fig 3.1d. The flapping frequency of the raw data of about 12.3Hz can be clearly seen from the peak in the FFT curve in Fig 3.1e where another peak is at 50Hz (noise). The flapping is started a few seconds after the data has already started being recorded. This can be seen from a low band and then the high fluctuations over it as the flapping starts.

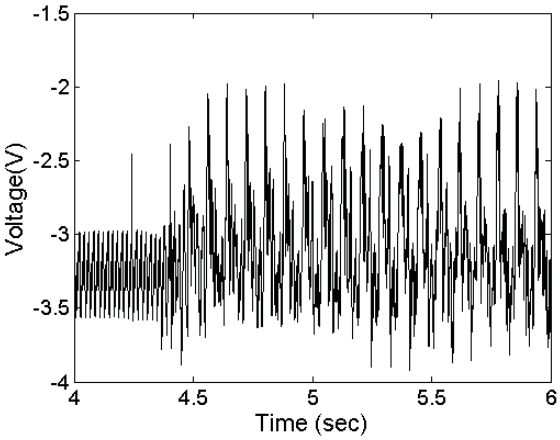

Figure 3.1 (a). Raw Data from the load cell for 1X wing (Model 1) at 12.3 Hz

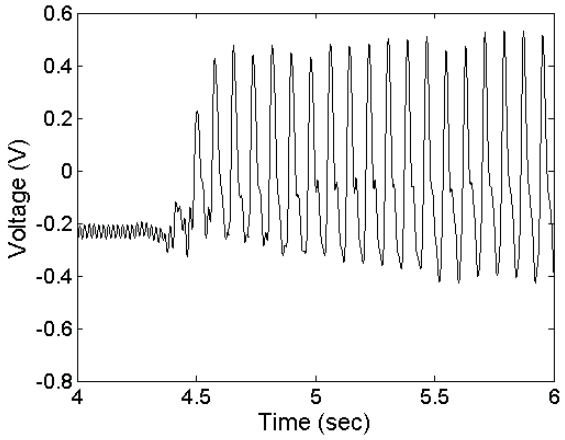

Figure 3.1 (b). Data after filtering frequencies over 25 Hz

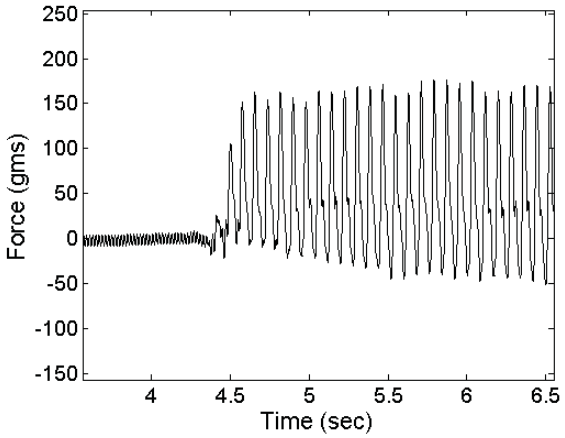

Figure 3.1 (c). Lift Vs Time data after multiplying filtered data by calibration coefficient and shifting it to zero level.

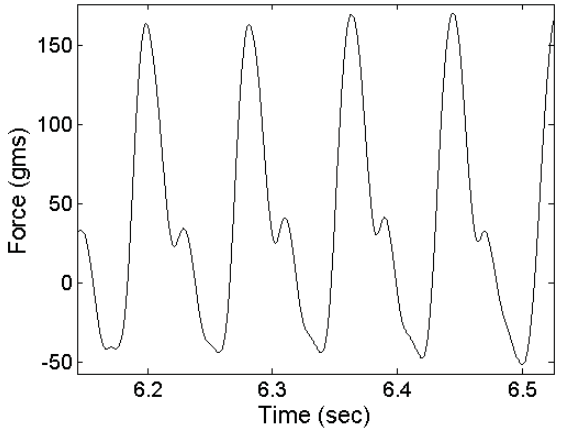

Figure 3.1(d). Zoomed view of the data of Fig 3.3(c)

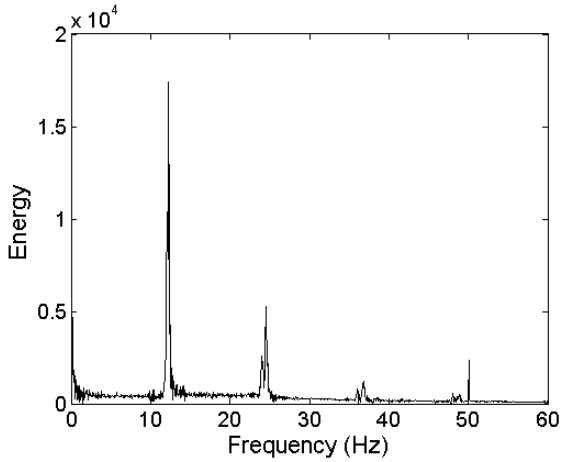

Figure 3.1 (e) FFT of the filtered data, peak of 12.3 Hz clearly seen.

Finally these values of lift and drag vs frequency and the corresponding lift and drag coefficients are plotted as shown in Fig 3.2-3.7. The following plots are for model 1 with various wing sizes.

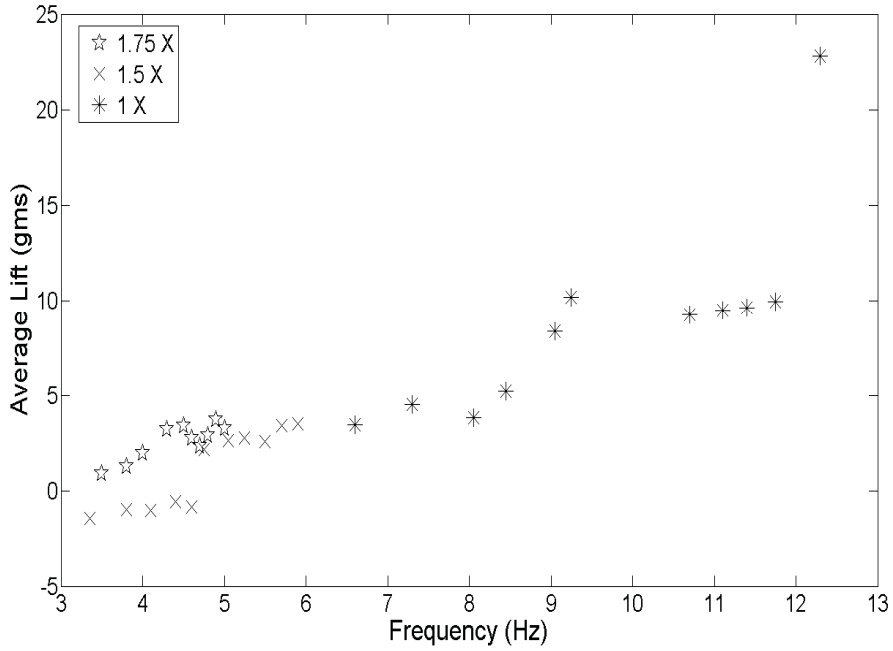

Figure 3.2 Average Lift Vs Frequency (For Model 1)

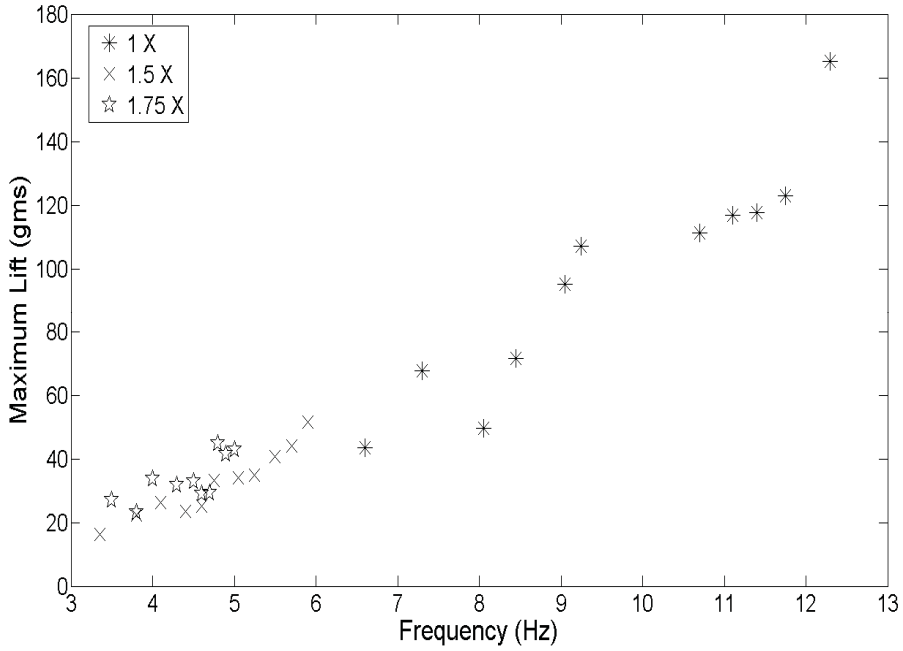

Figure 3.3 Maximum Lift Vs Frequency (For Model 1)

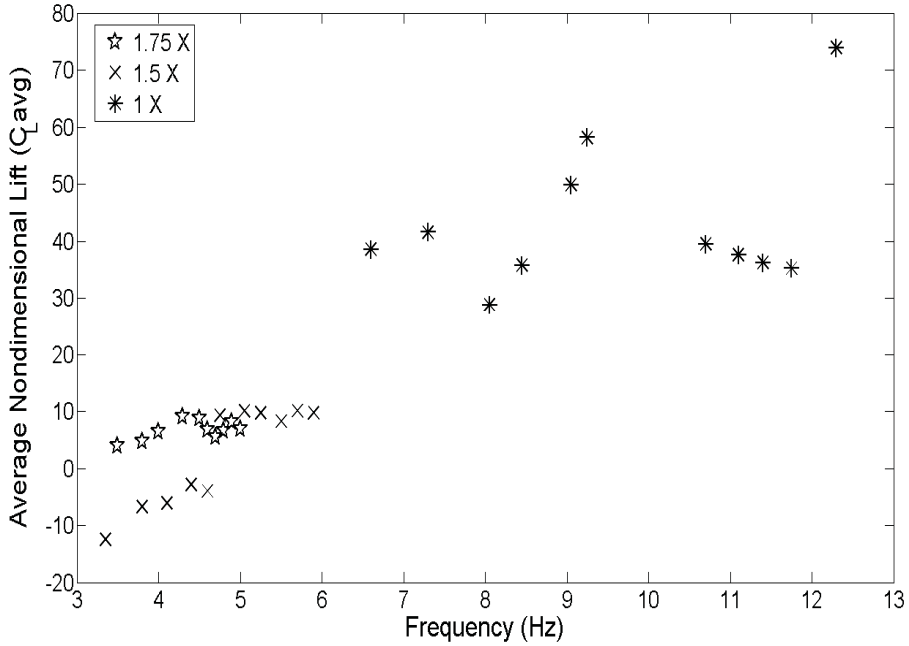

Figure 3.4 C_L avg Vs Frequency (For Model 1)

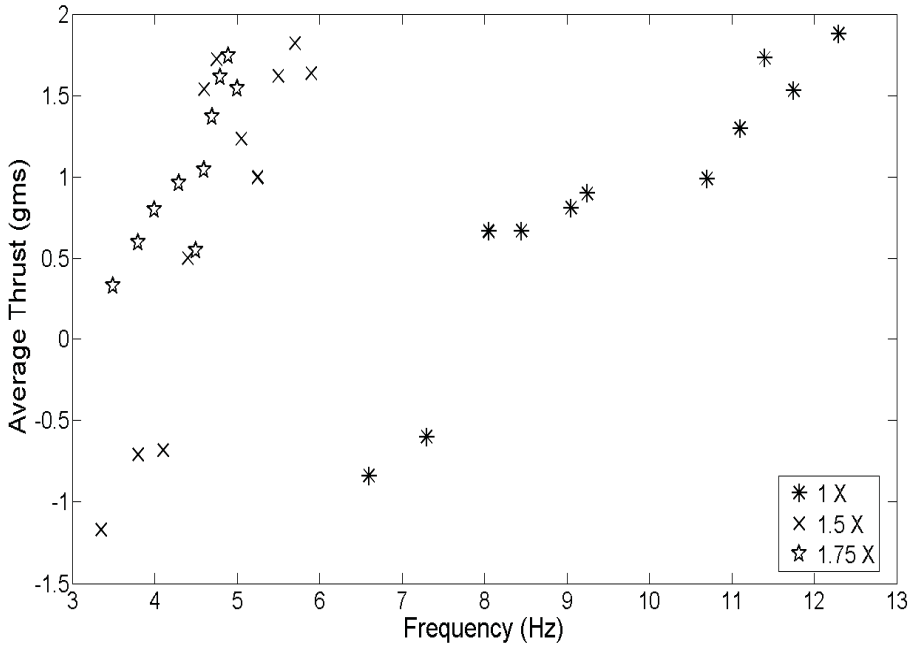

Figure 3.5 Average Thrust Vs Frequency (For Model 1)

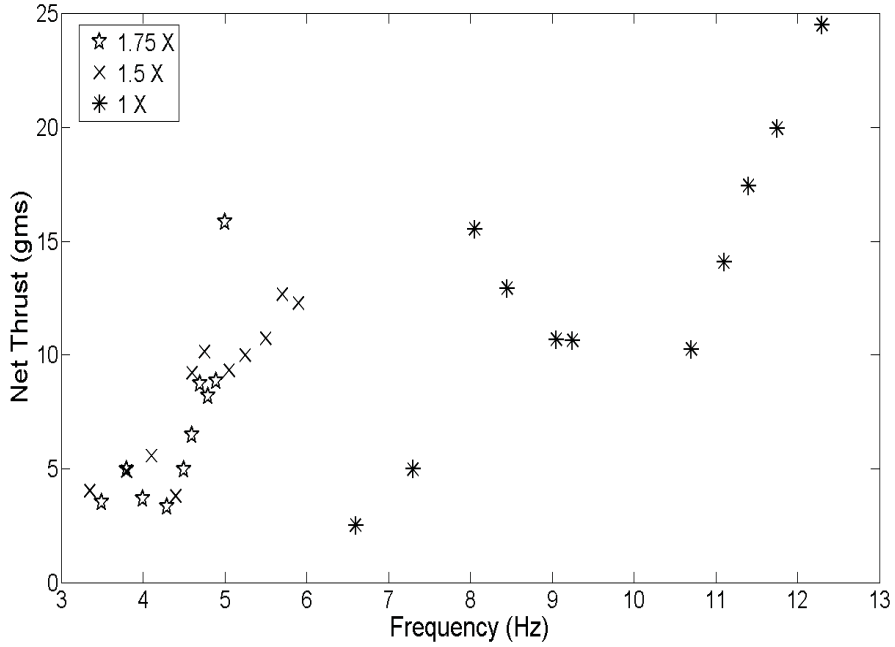

Figure 3.6 Net Thrust Vs Frequency (For Model 1)

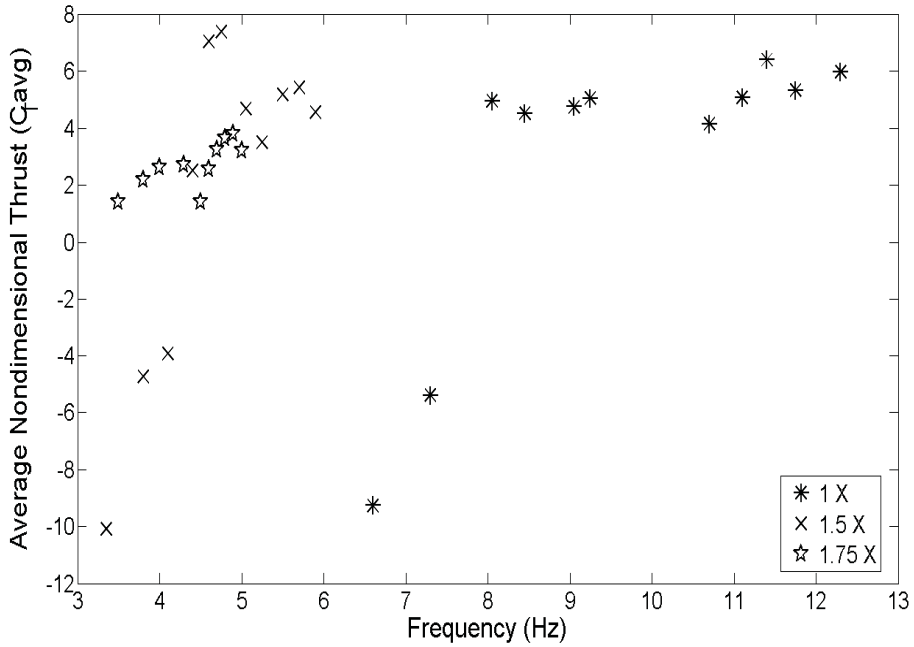

Figure 3.7 C_T avg Vs Frequency (For Model 1)

From Fig 3.2, 3.3 and 3.4 it is clear that lift is definitely a function of frequency. Though there is gap between the frequencies of 1X model and the rest, still it looks like if the frequency would have been the same the lift forces would have been quite nearer. Though the lift may not be exactly equal to the 1X model, as the clapping effect is more pronounced in the 1X model, leading to sustaining of lift even in the upstroke (discussed in the PIV results), but yet the peak of maximum lift forces in the downstroke of other wings owing to their bigger span supersedes the 1x model provided they are at the same frequency of flapping. But due to effective clapping by the relatively smaller wing the net lift increases with decreases in wing size. Thus the effect of frequency is well pronounced on the lift produced. The average lift or the net lift can be increased by decreasing the negative lift generated in the upstroke (by effective clapping) or by increasing the positive lift in downstroke. Former way can be achieved by relatively smaller wing (as the relation of size and clapping is already discussed in PIV results) and hence by more effective clapping, whereas the latter way is achieved by increasing the frequency or to be precise by increasing the tip velocity and hence the Re.

It is quite evident from Fig 3.5 and 3.6 that thrust don't show similar response to wing size and frequency as that of lift. It increases in the same way for all the wings irrespective of the range of frequencies that they are operated with. It can be seen that for the same range of frequencies of 1.5X and 1.75X, the thrust is more for 1.75X. This indicates that it is more a function of tip velocity, thus on the combination of frequency and span both. As discussed in the PIV results that thrust forces are predominantly generated during the stroke reversals. Hence the magnitude of thrust is expected to depend on the vortex interactions during the stroke reversals. This depends on the

strength of the interacting vortices, which in turn depends on the tip velocities and hence on Re. thus with the same tip velocities and Re range the thrust generated will be similar. The same can be seen from Fig 3.5 and 3.7 where the thrust of 1.75X at lower frequency is almost equal to the thrust of 1X at higher frequencies. This is because the thrust depends not on frequency alone but wing span as well. So it's the product of both the parameters that determines the thrust. With more feathering effects of a wing, the contribution to thrust increases. This amount of feathering in our wings depends on the size as discussed earlier (it increases with wing size). Thus the thrust forces calculated for model 1 are more dependent on wing size than on the frequency. The same is also seen by the thrust calculations done by PIV data in the next chapter. So the behavior as shown in the force data is quite expected and verified for model 1 by comparing through the PIV data.

As the source and mechanism of generation of lift and thrust are different, hence their behavior and response to the parameters like frequency and wing sizes are different. As discussed in the PIV results that the lift depends on the tip velocity and the strength of vortices over it, as well as on the effective clapping it undergoes towards the end of the upstroke. So its dependence on the frequency becomes very prominent. Thrust is seen to be generated mainly during the stroke reversals due to the ejection phenomena. The strength of ejected jet does depend on feathering angle as well as the interacting vortices' strength which in turn here depends on the size of the wing and the tip velocity respectively for model 1. Thus thrust dependency with wing size is more observed than its dependency on the frequency. It is seen to be linear with wing span, whereas the lift dependency on the frequency is more dominant and here it is inversely varying with wing size (due to the effective clapping action).

Thus the nature of force data when justified with flow structures using PIV gives an idea of occurring mechanisms and the aerodynamics behind it. Even though the justifications and mechanism of flapping wing flight will change along with the type of wing, model or the forward velocity range (J range). But for the model used in the experiments in the unsteady regime with low Reynolds number, the basic aerodynamics is observed and noted out.

There exist some chances of errors in the force data calculated from the load cell experiments. As the whole model is placed over the load cell the motor vibrations or the hammer blow of the vibrating cg of the model which may not be eccentric with the column of the load cell. So due to all such unwanted factor the forces calculated from such experiments can be in the higher end. But yet the trend of such forces has to be the same. So if we are getting more values of the force than the actual that is produced by the wing itself then the measured value of forces will be towards the greater end in every experimental result. All the motor vibrations and eccentric effects will also grow with the flapping frequency. So the nature of variations of the forces produced actually by the wings will be the same as predicted here. Though the values may be a little different than what is shown, but the pattern and nature of the plots will still be same.

For model 3 only lift measurements are done to view the effect of lagging. The experimental procedures and load cell being the same, only the new model is placed on the load cell and all other procedures are same. The effect of lead lag motion is observed from Figure 3.8-3.10. Only 1.75X wing is tested on the model.

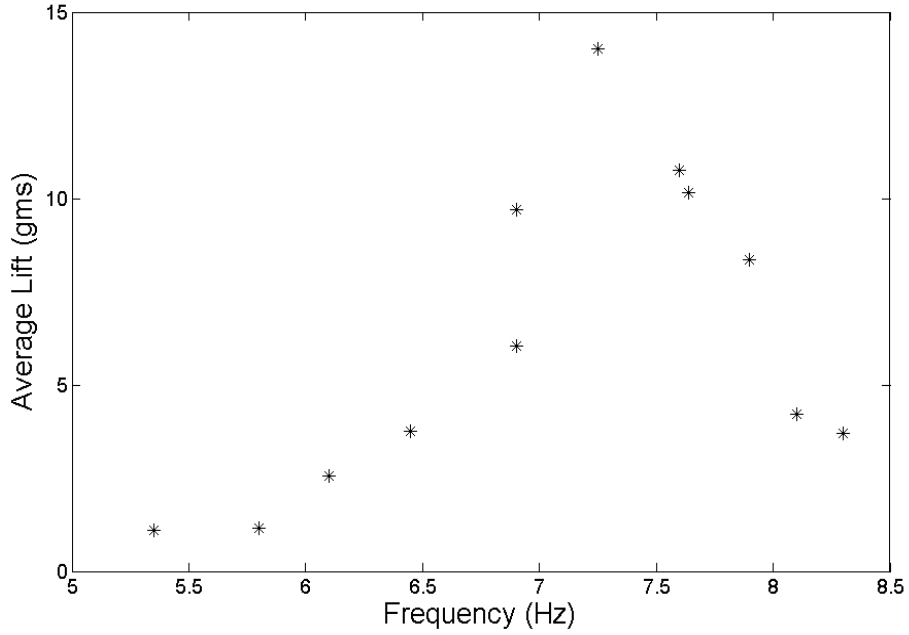

Figure 3.8 Average Lift Vs Frequency (For Model 3)

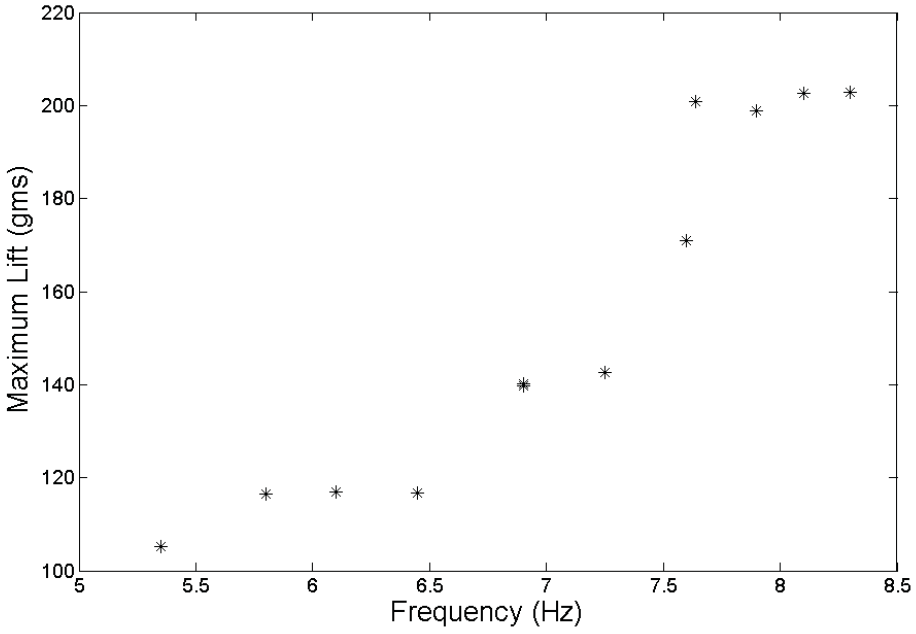

Figure 3.9 Maximum Lift Vs Frequency (For Model 3)

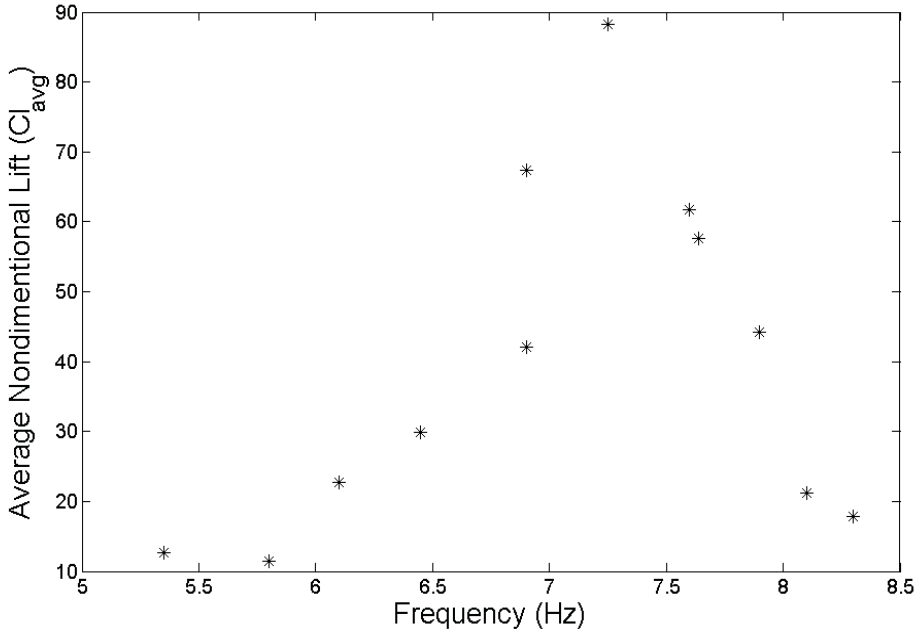

Figure 3.10 C_L avg Vs Frequency (For Model 3)

At varying J values

Apart from the butterfly shaped wings three rectangular wings of different aspect ratios (AR=1.5, 2 & 3) are tested on model 1 for better understanding of the shape dependence of the wings on the forces generated. The experiments are conducted in a wind tunnel where the forward air velocity is varied between 0.4-1.85 m/s. 1.75X butterfly shaped wing is only tested for this case as it matches the same span length (R) with the other rectangular wings. Experiments are also conducted with model 3 but with only 1.75 X wing to find out the difference in the nature of forces due to its lead lag motion.

Lift and thrust variation with J (Fig 3.11-3.12) for all wings on model 1 show that the coeffiecients drop with increasing J values. In other words higher lift and thrust coefficients can be obtained for lesser J values. Another thing that can be observed here is that the rectangular wing with AR=2 gives the best lift and thrust among other rectangular wings. The notion here is that with increase in AR, the chord becomes much smaller as compared to the span of the wing making it more rigid. Thus lower AR values make the wing more flexible. With enhanced flexibility lift decreases but thrust increases at a particular J value. This leads to an optimum flexibility of the wing corresponding to a particular AR which would give an optimum value of higher lift and thrust both. Another thing worth mentioning is that with same J value the butterfly wing of 1.75X gives both better lift and thrust showing a shape dependency on the forces or flow physics which we plan to study later.

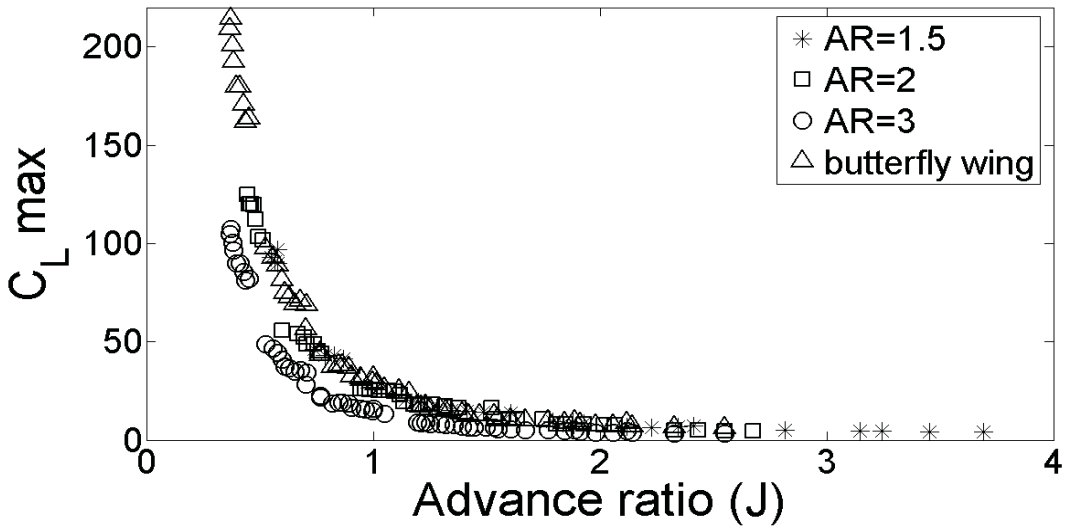

Fig 3.11 Lift coefficient (C_L) vs advance ratio (J) for the tested wings on model 1

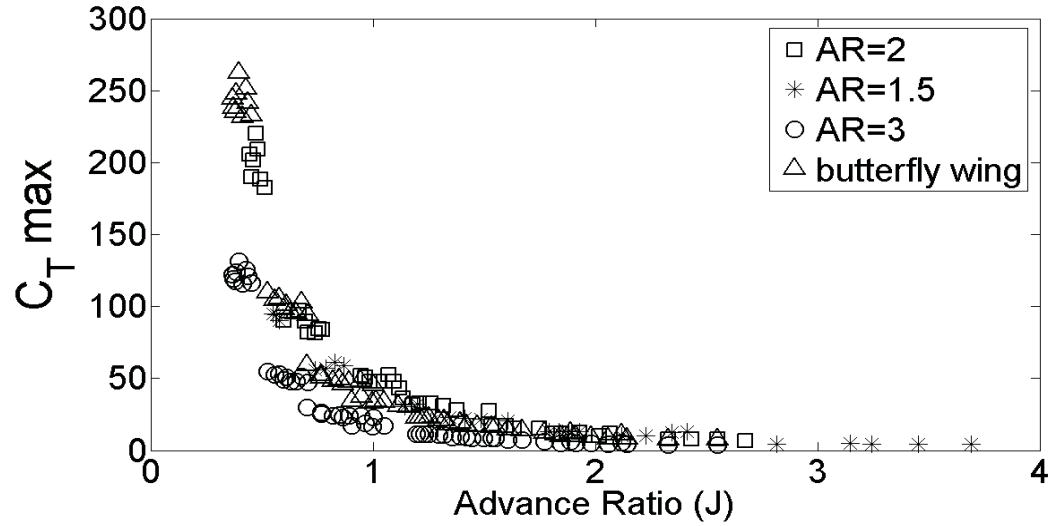

Fig 3.12 Thrust coefficient (C_T) vs advance ratio (J) for the tested wings on model 1

As already concluded earlier that both lift and thrust increases with frequency or the encountered Re number. In Fig 3.13-3.14 the variation of C_L and C_T with frequency at different Re numbers and at different J values are shown. Here it is found out that for any wing flapping at a certain frequency the better coefficients are obtained at lower Re values or at lower J values. This puts into light why insects have higher coefficients than birds as they have much lesser J values of flight.

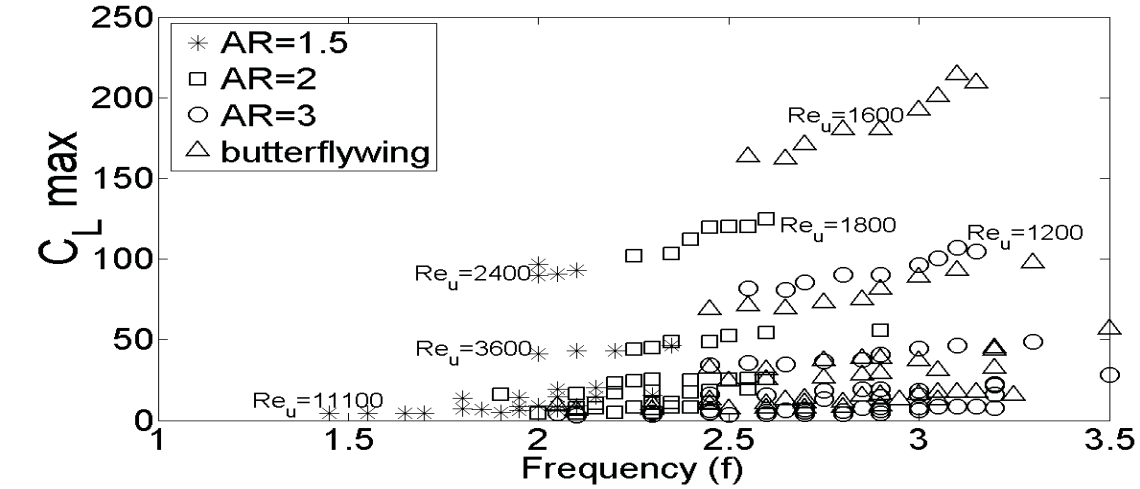

Fig 3.13 C_L vs flapping frequency for all wings at different J and Re values on model 1

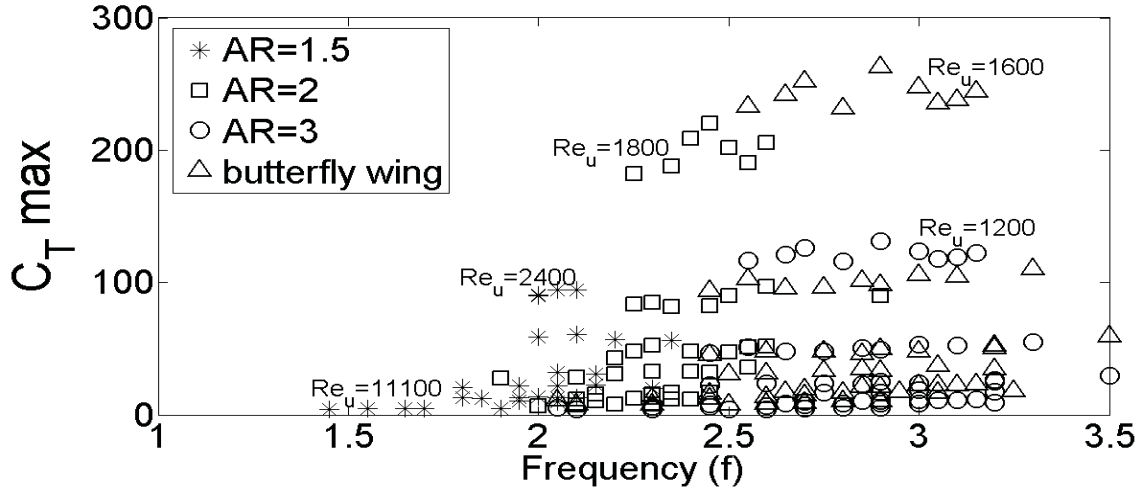

Fig 3.14 C_T vs flapping frequency for all wings at different J and Re values on model 1

Maximum C_L (rotational) vs f (Fig 3.15) shows that the rotational component of lift decreases with increases in flapping frequency or flapping velocity of the wing. The rotational effects at a particular frequency increases with flexibility thus wings with low AR values have higher lift coefficients at the same frequency. Similar conclusion for the rotational contribution of thrust is also found (Fig 3.16). But in the rotational contribution of thrust the wing with the most flexibility has higher values at a particular frequency. Here the rotational contribution of lift is more a property of the wing and is almost independent of the forward wing velocity.

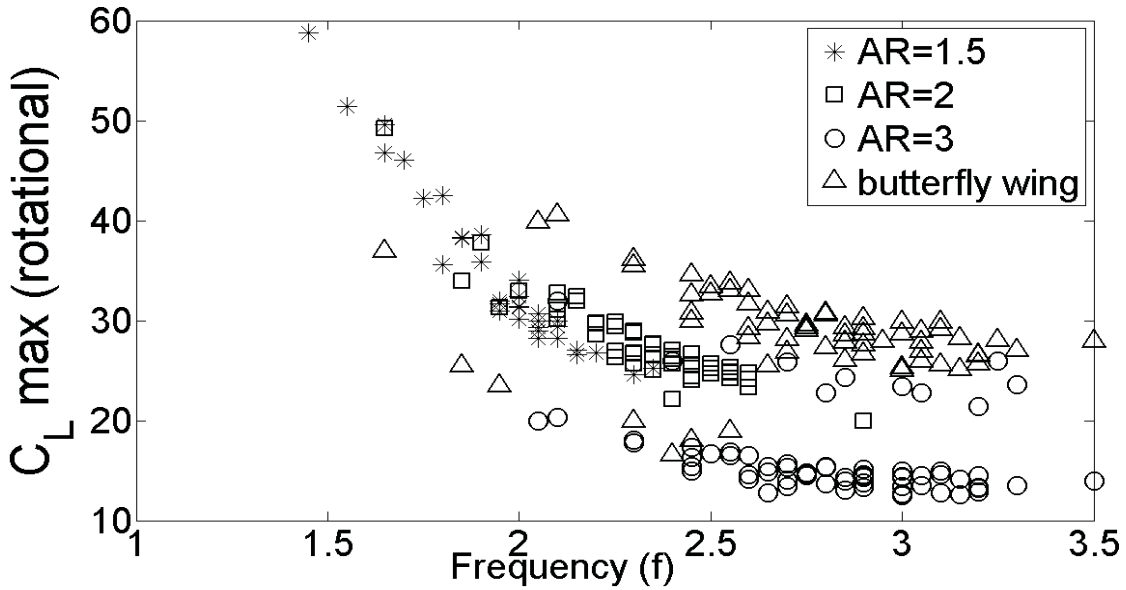

Fig 3.15 Maximum C_L (rotational) vs flapping frequency for the wings on model 1

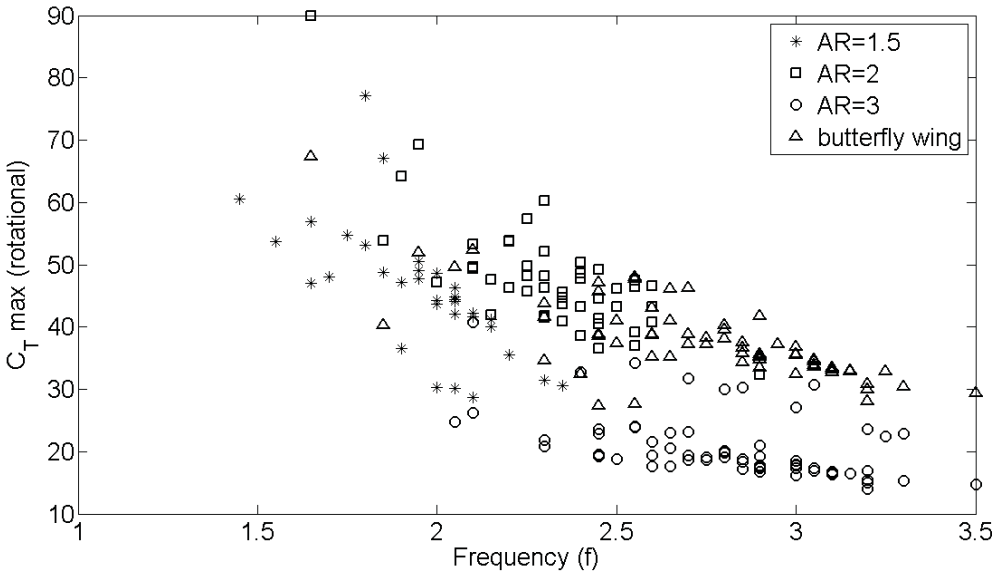

Fig 3.16 Maximum C_T (rotational) vs flapping frequency for the wingson model 1

For model 3, the experiments are done with 1.75X wing only to understand the effects of lead lag motion and the results are plotted in Fig 3.17-3.22. We see here that both the lift and thrust coefficient with advance ratio follow the same trend with both the models. However the values of these coefficients are higher with model 3. Again important point worth mentioning here is that the roational coefficient of lift increases with frequency for model 3 unlike model 1 suggesting its higher contribution to the total lift with feathering and lead lag effects. Rest other parameters behaviour is similar to the model 1 results with obtaining higher coefficients at lower Re.

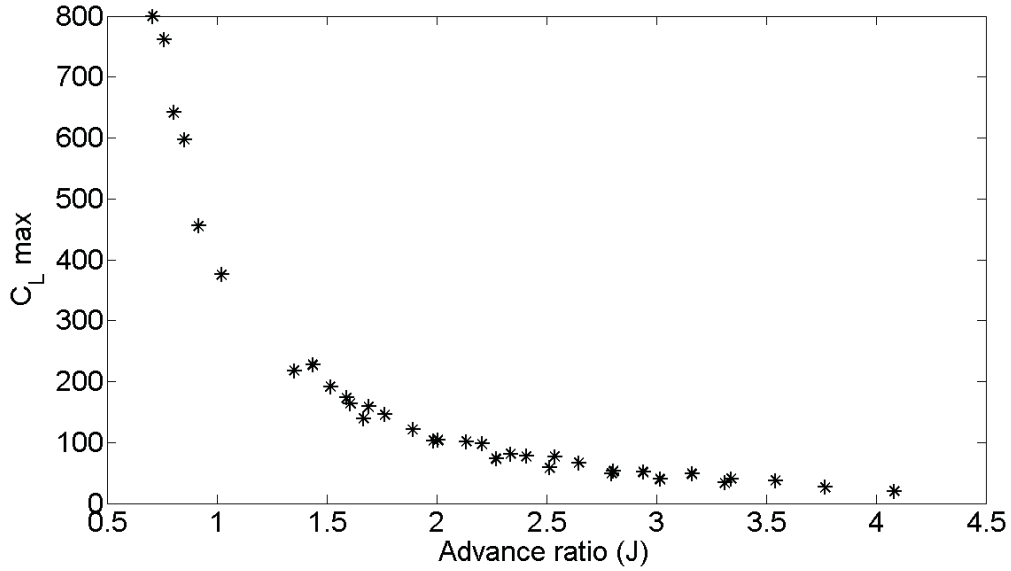

Fig 3.17 Lift coefficient (C_L) vs advance ratio (J) for 1.75X on model 3

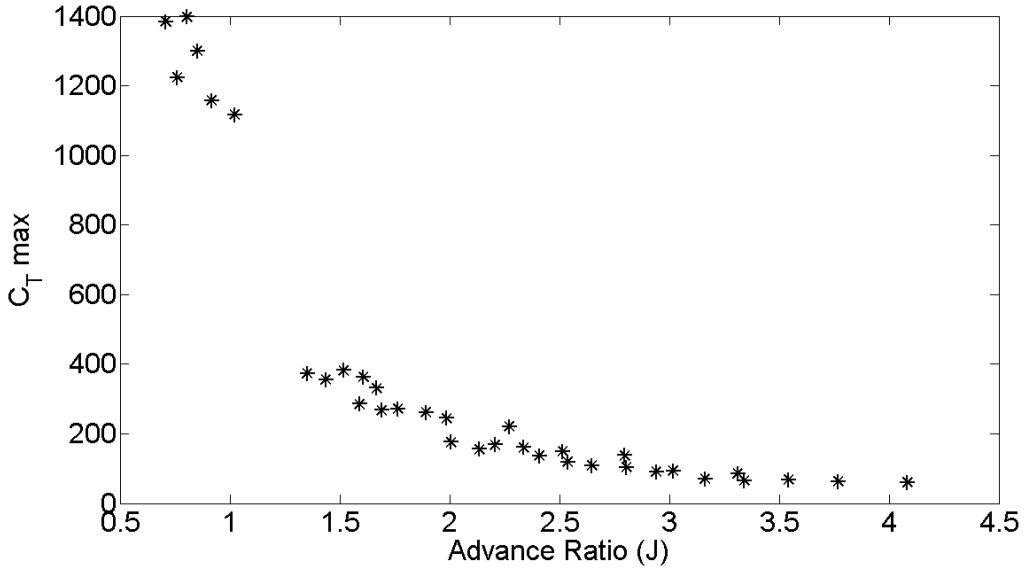

Fig 3.18 Thrust coefficient (C_T) vs advance ratio (J) for 1.75X on model 3

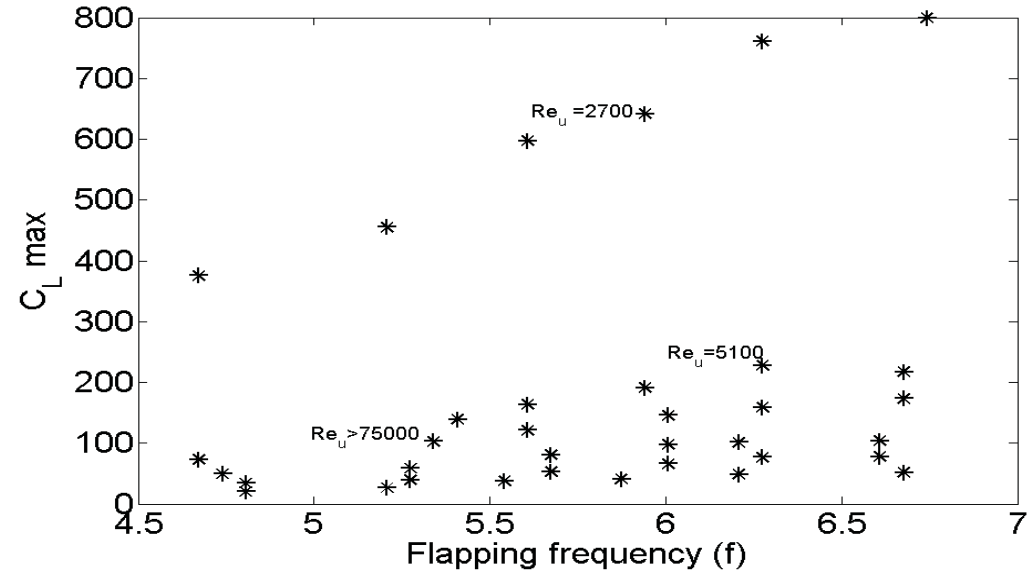

Fig 3.19 Lift coefficient (C_L) vs flapping frequency (f) for 1.75X on model 3

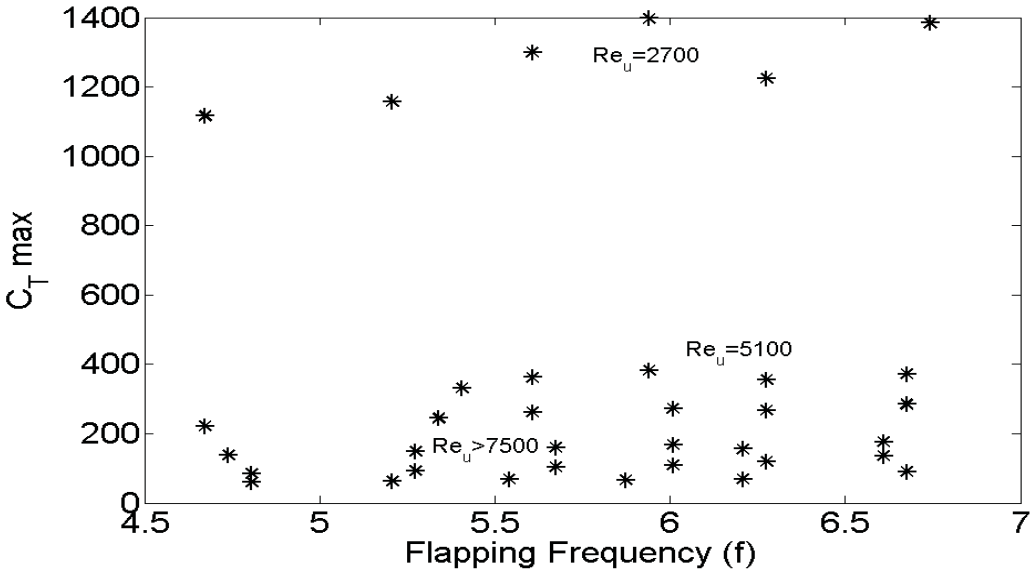

Fig 3.20 Thrust coefficient (C_T) vs flapping frequency (f) for 1.75X on model 3

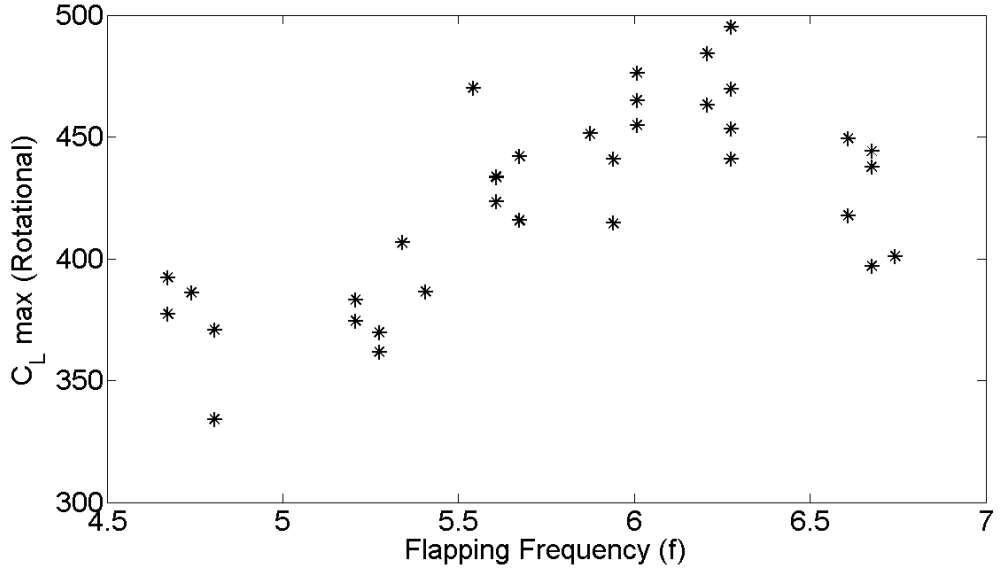

Fig 3.21 Rotational Lift coefficient (C_L) vs flapping frequency (f) for 1.75X on model 3

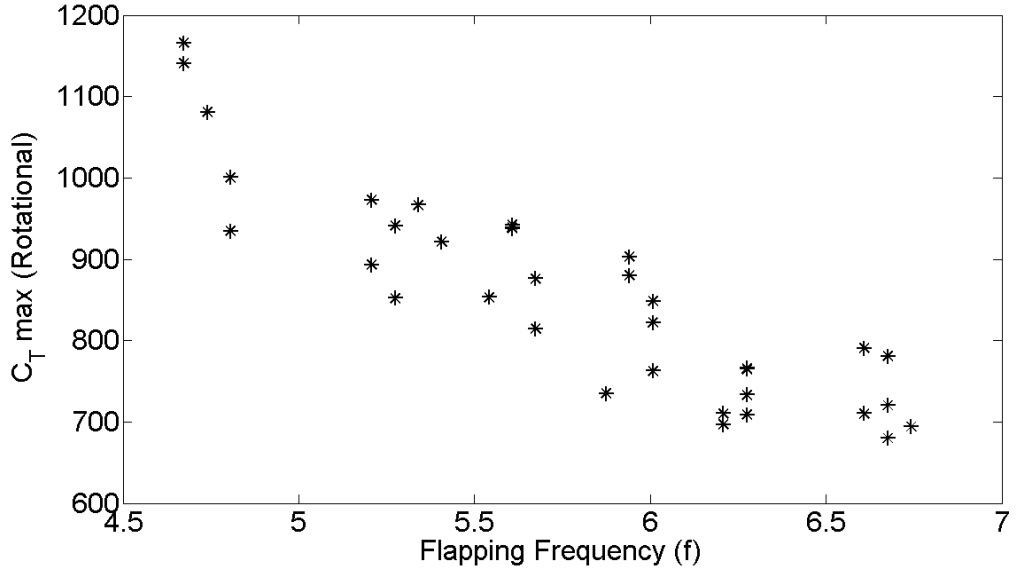

Fig 3.22 Rotational thrust coefficient (C_T) vs flapping frequency (f) for 1.75X on model 3

4. PIV Measurement

4.1 Experimental set up

The experiments are carried out in a closed chamber of glass or thermocoil depending upon the size of the model as a whole. Model 1 is fitted with monarch butterfly's scaled wings (Fig 1.3). Measurements are carried out in cross-sectional planes along the chord of the wing in different spanwise locations. The flapping frequency is kept constant (4Hz for 1.75X, 6Hz for 1X wing) during experiments at different sections. The size of the wing is varied on the insect model to study the effect of size and the frequency of flapping. As the wings are connected by linkages to a dc motor, the current and voltage supplied to the motor are kept constant, thus the change of wing size automatically changes the frequency of flapping at the same time.

A double pulsed Nd: YAG laser (Quanta system, 200mJ/pulse, 10Hz) is used for illuminating the flow field. PIV mmeasurements are carried out at 10Hz acquisition frequency.The enclosed chamber is filled with smoke containing the seeding particles. The size of the seeding particles is $\approx 1\mu m$. The time between the two laser pulses is kept as $978\mu s$ for measurements. A Nanosense Mk III (1000 frames/sec, 1280x1024 resolution) camera is used for capturing the particle images, run in dual frame mode with the same timed delay as the two lasers. Laser and camera are synchronized by a timer box which is controlled by the computer software. The velocity and vorticity variations of the flow field are calculated for different experiments using Dynamic Studio software from DANTEC dynamics.

Though during the PIV experiments the smoke containing the seeding particle may have some forward velocity depending upon the way of applying it, yet it is negligible enough to be accounted for in the short span of the experiments performed. To overcome the chance of smoke having some forward velocity, some settling time has been kept for the smoke to get stabilized in the chamber containing the model, before the measurements are finally done. Thus the unsteady regime can be ensured. The smoke quantity, the settling time and the way of putting it is purely based on hit and trial and after finding the best possible way, the same is repeated for all the experiments of PIV.
Measurements are taken at 3 sections at the wing. For the 1X model, the measurements are carried out at 0.2R, 0.3R, and 0.5R respectively from the tip of the wing, where R is the single wing span (Fig2.1). For the 1.75X (1.75 times the size of 1X model) measurements are taken at 0.3R, 0.4R, and 0.6R respectively from the tip of the wing.

Similarly for model 2 the PIV measurements are carried out to see the similarities in flow field and only the analysis of thrust variation is done for this case.

Further for model 3 using 1.75X wing PIV experiments are performed at 5Hz flapping frequency. For better insight into the difference due to lead lag motion the experiments are conducted at the aquisition frequency of 500Hz with the time between the two frames being 2ms. For this particular experiment a different laser is used (quantronix 20mj/pulse, 1 KHz) to get a higher aquisition rate.

4.2 Results

2D results

Experimental results obtained from measured velocity and vorticity field using PIV are presented in this section. Analysis and comparisons are made for each stroke positions for the 1X and 1.75X wings of model 1. The measurements are taken at 3 locations of these wings. For the 1Xmodel the measurements are carried out at 0.5R, 0.7R and 0.8R from the root of the wing, where R is the span of one wing (Fig 1.3). For the 1.75X wing measurements are done at 0.4R, 0.6R and 0.7R from the root of the wing. The sequence of flow visualization images, velocity and vorticity field data is presented at 0.4R spanwise location for 1.75X wing sizes (Fig4.1). The velocity and vorticity levels are shown adjacent to the corresponding PIV images. The results of both the wings are compared to understand the variation of flow properties with frequency and wing size. The flapping frequency is kept constant for a wing during measurements (4Hz for 1.75X wing, 6Hz for 1X wing). The mechanisms and the typical flowfield are discussed in details for one sequence.

All the experiments are carried out at zero forward velocity (J=0), which implies that the study regime is completely unsteady. The effects of underlying vortices and their subsequent interactions in both the strokes have been observed. The role of ejection (Fig 4.4) and their timing during the stroke reversal have been observed (Fig 4.5). The wing kinematics during the stroke reversal is found to be very crucial as the wing rotation or twist plays a significant role in the generation of lift and thrust forces. This rotation or twist of the wings plays a great role in the large scale lift generation. The PIV results of the flapping cycle are shown for 1.75X wing at 4Hz at 0.4R from the root of the wing (Re=8060) in Fig 4.1-4.7, the start of downstroke is conventionally taken as t/T=0. The velocity and vorticity fields are shown for PIV results.

The blue color shows the LEV as clockwise (negative vorticity values) as from the direction the wing is seen the leading edge is on the left side. Similarly the TEV is in red and yellow color as the circulation is anticlockwise (positive values). The growth and evolution of LEV and TEV is clearly seen in 4.1-4.3. This attached LEV is believed to be one of the important factors in the lift production in flapping flight and even at higher angle of attack as it delays the stall. As there is no forward velocity in the experiments performed, the LEV and the TEV are connected and forms a single structure which runs over the whole periphery of the wing. The vorticity levels of LEV and TEV can be seen to be equal and opposite at all positions of the downstroke and even at different locations in accordance with Kelvin's conservation of circulation. This low pressure zone over the wing produces a high lift and a little thrust depending upon the orientation of the wing at that point of the stroke.

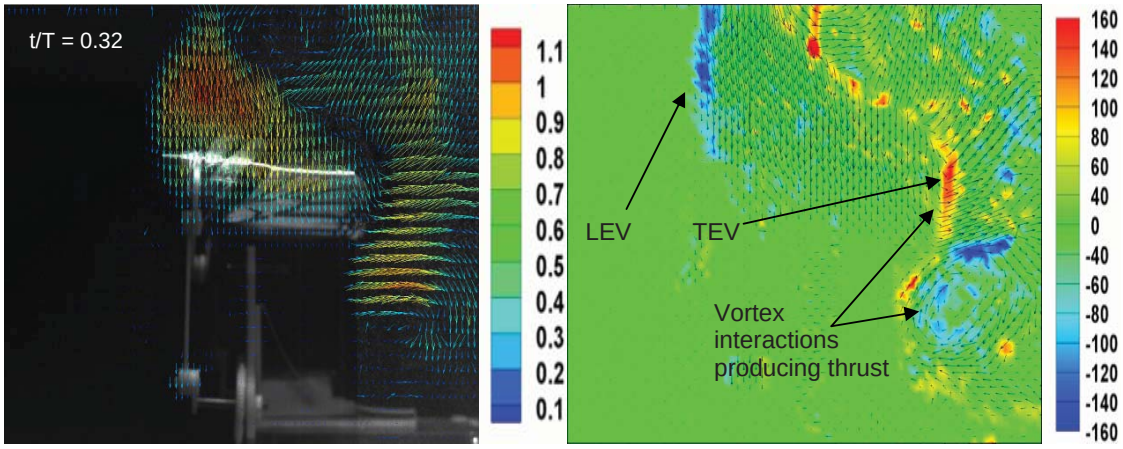

Fig 4.1 Beginning of downstroke, formation of LEV and TEV, production of thrust due to vortex interactions at the trailing edge; velocity and vorticity fields

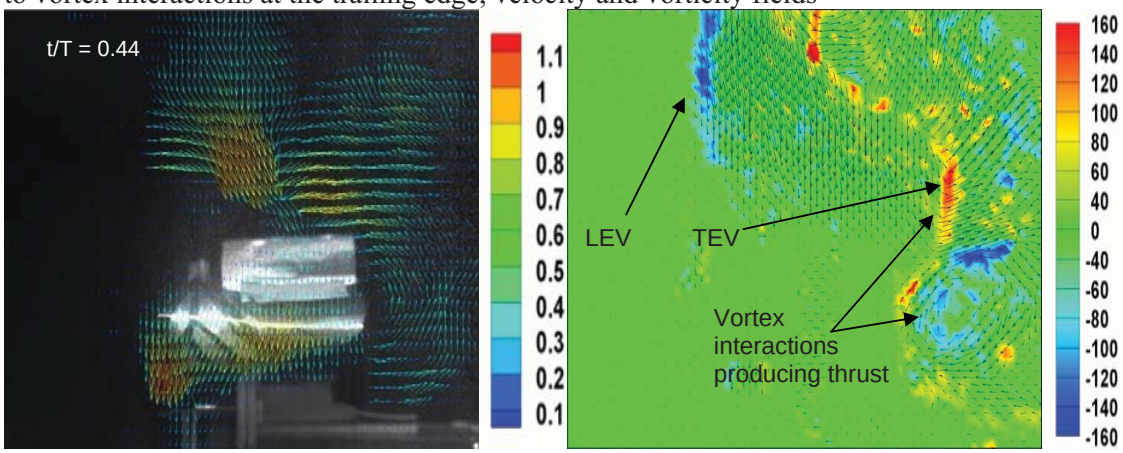

Fig 4.2 Growth and evolution of LEV as downstroke progresses; velocity and vorticity fields as the the stroke progresses, the strength of LEV as well as TEV increases as can be seen from the vorticity levels

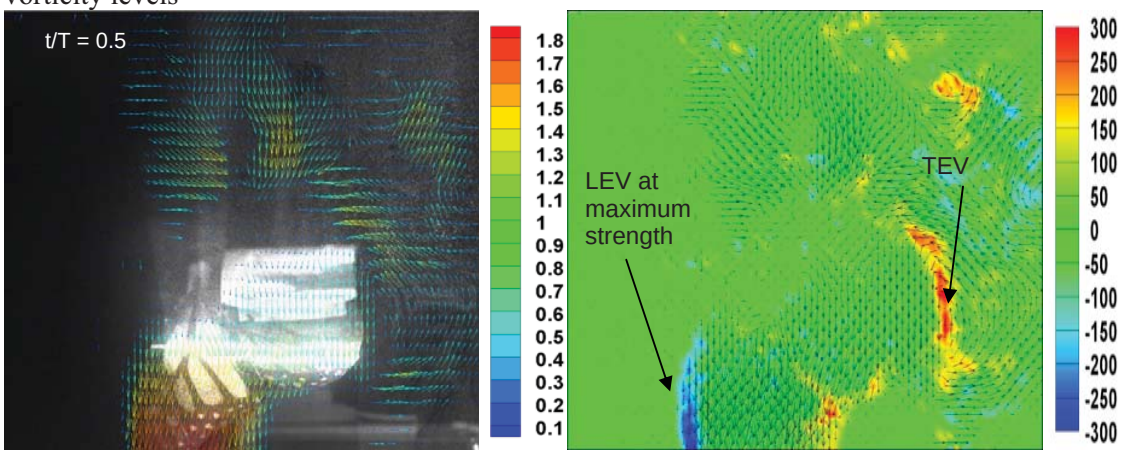

Fig 4.3 End of downstroke the strength of LEV reaching maximum; velocity and vorticity fields

As the stroke changes from downstroke to upstroke, due to the opposite motion of the wing another tiny vortex develops below the wing as shown in Fig 4.4. This vortex (which is of opposite circulation to that of the TEV) is small in size and strength, as compared to the TEV at this point of the stroke. The TEV interacts with this vortex (Fig 4.4) and both being closer to each other, the induced velocities on each other is high. As a result both the vortex pair is ejected at a very high velocity along the trailing edge satisfying the Kutta condition (Fig 4.5). Even before ejection of these vortices pair due to there mutual interaction, the fluid in between these two vortices gains momentum due to the induced velocity. Because of the ejection of fluid as a jet and the vortices as a pair, a high momentum is in turn imparted to the wing as per the momentum conservation. This results in a high amount of force in the opposite direction of the ejection, on the wing. This ejection moving downwards in well visualized in Fig 4.6.

As the upstroke progresses the vortices of opposite circulation to the earlier LEV and TEV pair grow below the wing (Fig 4.4-4.7) thus, creating a downward force on the wing but an increase in the subsequent thrust generation due to the feathering resulting in momentum transfer at an angle which resolves finally to downward force and thrust in two perpendicular directions. After the ejection along with the jet, the vortex pair (Fig 4.6) doesn't vanish downstream rather is reutilized in the suction due to upstroke in Fig 4.7. This phenomenon is termed as wake capture and it is well observed that the pair of vortices just shed away at the stroke reversal at early of upstroke is reutilized in the suction of the wing in absence of any forward velocity.In case of non-zero advance ratio the same phenomenon is observed with varying strength if the advance ratio, $J < 1$ and flapping frequency is high. Thus the wake capture is possible if the stroke reversal is faster than the speed at which the ejection occurs. It is conjectured that the same mechanism may be used by the insects in their advantage for maneuvering.

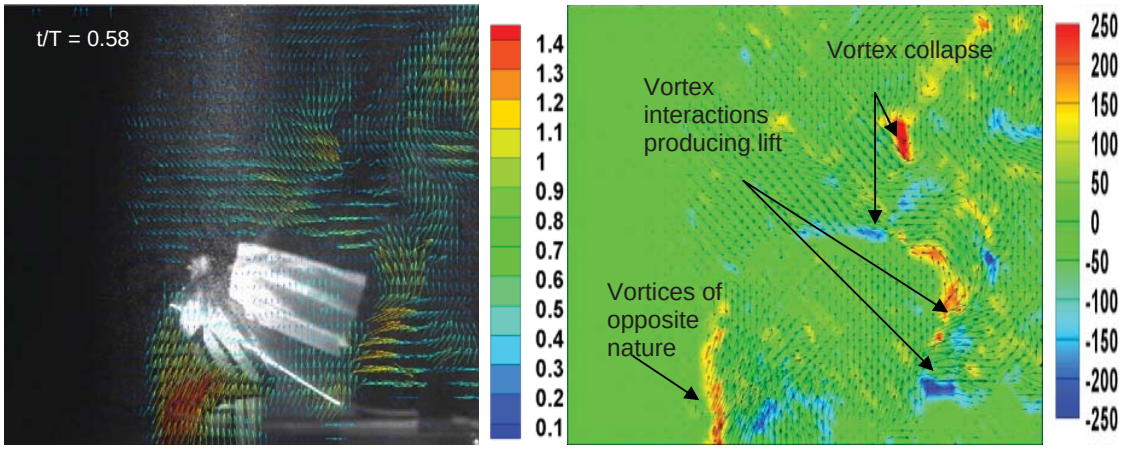

Fig 4.4 Start of upstroke, thrust and lift generation due to interacting vortex pair at the trailing edge; velocity and vorticity fields

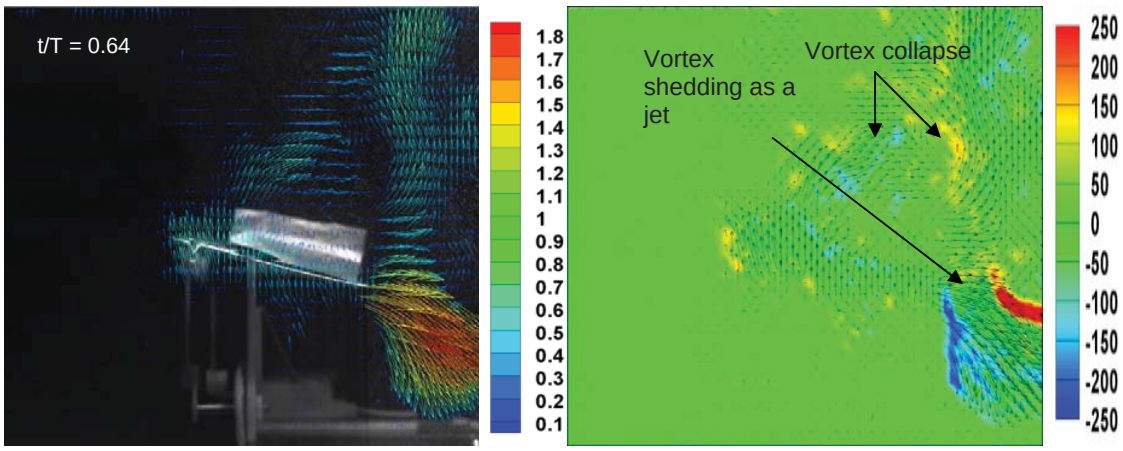

Fig 4.5 Ejection of the vortex pair due to their self induced velocities resulting in high lift and thrust, the contribution to each depending on the feathering angle at this position of the wing; velocity and vorticity fields

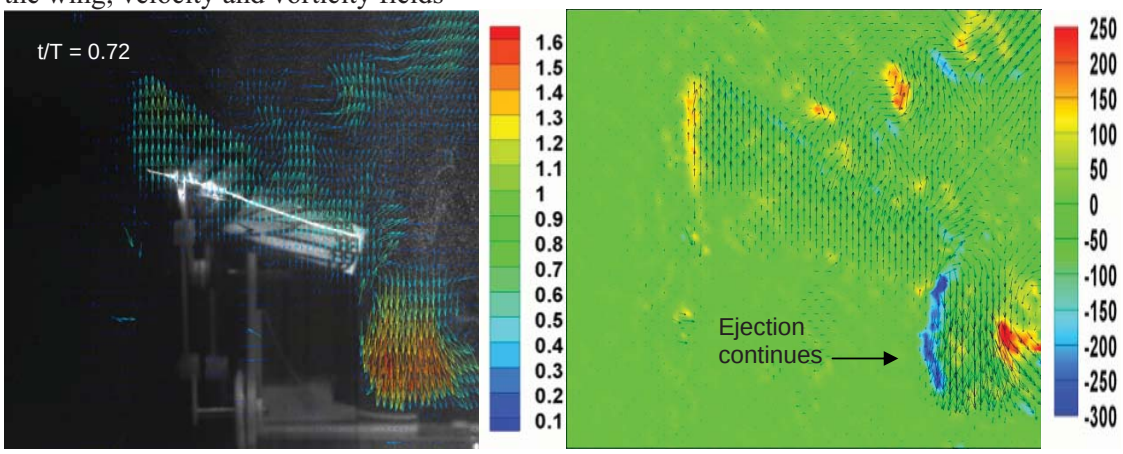

Fig 4.6 Vortex pairs ejected previously are still visible in the wake later in the upstroke; velocity and vorticity fields

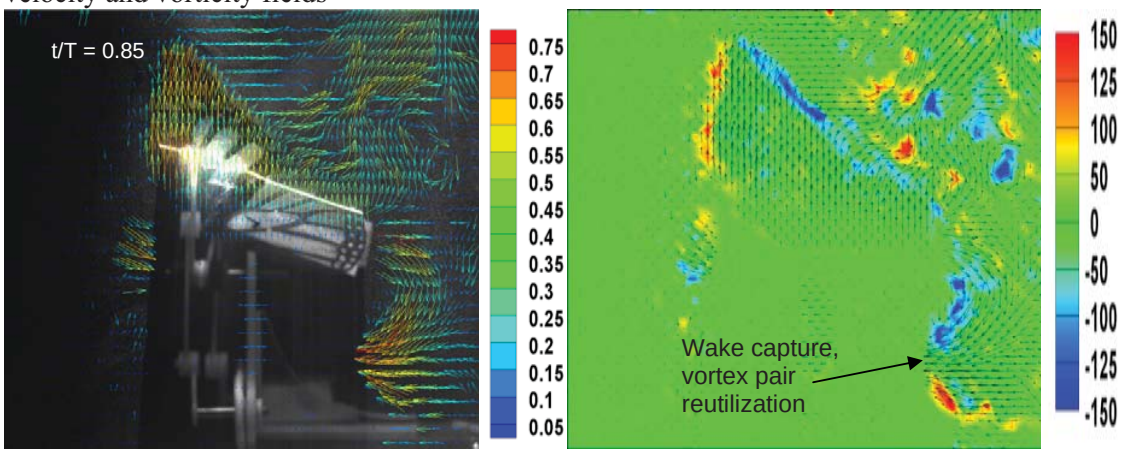

Fig 4.7 Reutilization of the ejected pair, due to the suction created during the upstroke, producing some lift even in the upstroke; velocity and vorticity field

In Fig 4.8 it can be seen that the maximum vorticity of LEV grows as we move from the root of the wing to the tip. Which is the effect of sectional velocity of the wing, V = 2ΦfR. In Fig 4.9 the nondimensionalized maximum vorticity (ωc/V) is plotted with nondimensional time. It shows that the vortices grow with time and the nondimensional maximum vorticity occurs at an optimum location where the velocity is high and chord is sufficiently large. It depicts the possibility of LEV of class II (the strength and size is more or less uniform along the wing and thorax of butterfly) only near the tip of the wing where the chord variation is large (Fig 1.3). Non dimensional vorticity depends on chord length (c) as well as the flapping velocity (2ΦfR) (eq 2). Thus it may so happen that the vorticity increases towards the tip of the wing but yet again the chord length also decreases towards the tip. The total value of this product of vorticity (which increases towards the tip) and the chord length determines the net strength of the LEV. Depending upon the model or the wing geometry in particular the nature of LEV will change. The LEV of class III which states that the size and strength of LEV grows towards the tip of the wing should be observed in the most part of the wing where the chord is almost constant.

Sectional Reynolds number Res=2ΦfRc/ν (1)
Non dimensional vorticity = ωc/2ΦfR (2)

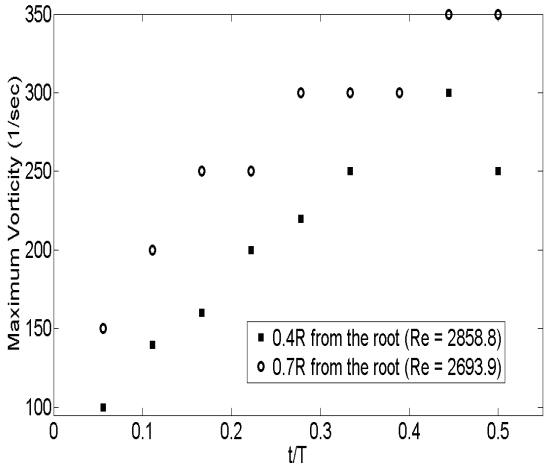

Fig 4.8 Variation of maximum vorticity of LEV for 1.75X wing at different R values

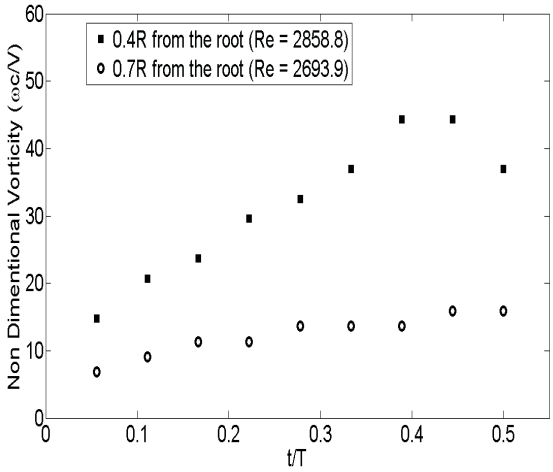

Fig 4.9 Non dimensional vorticity of LEV for 1.75X wing at different R values

From the observations it is interpreted that the strength of LEV depends on the sectional Reynolds number (eq1). The sectional Reynolds number of a wing cross section depends on the chord length at that cross section as well as the flapping velocity at that location. The physics and aerodynamics remaining the same, the difference in the nature is just attributed to the difference in the geometry or specifically the chord variation of the wing, which varies from species to species, or model to model.

The lift is generated mainly due to LEV, whereas the method for generation of thrust is entirely different. In the model 1 the thrust is generated during the stroke reversals due to Trailing Edge Vortex (TEV) pair interactions and their subsequent ejection as shown in Fig 4.4-4.5 apart from the thrust generated from the feathering of the wing in the total cycle. This ejection of the vortex pair (Fig 4.4-4.5) at the stroke reversals is responsible for thrust generation. The ejection depends on the Reynolds number and the contribution of this ejection on thrust or lift depends on angle of feathering, so both these parameters play a significant role. Thrust can be generated if there is change in the stroke plane angle with respect to body axis or by feathering motion.

Later the ejected pair is reutilized due to the strong suction in the upstroke as seen in Fig 4.7. This is termed as wake capture. This is observed in high frequencies or at lower J values as the time scales for ejection is less than the time scale of flapping. The wake capture is believed to be helpful in lift generation in the upstroke as the induced velocity helps in imparting some momentum and force in the upward direction to the wing.

The ejection timings for 1.75 X along flapping cycles at various frequencies are shown in Fig 4.10. It is evident that the periodicity and repeatability of the ejection at stroke reversals is maintained. The timings show that the ejection occurs around t/T=0.6 and the vortex pair is totally ejected leaving the trailing edge, passing down the wake for all the cases. This shows that the rotational twist at the stroke reversal or the feathering effect has a contribution to the timing of ejection apart from the Re. The feathering angle also determines the respective contribution of this ejection to lift or thrust.

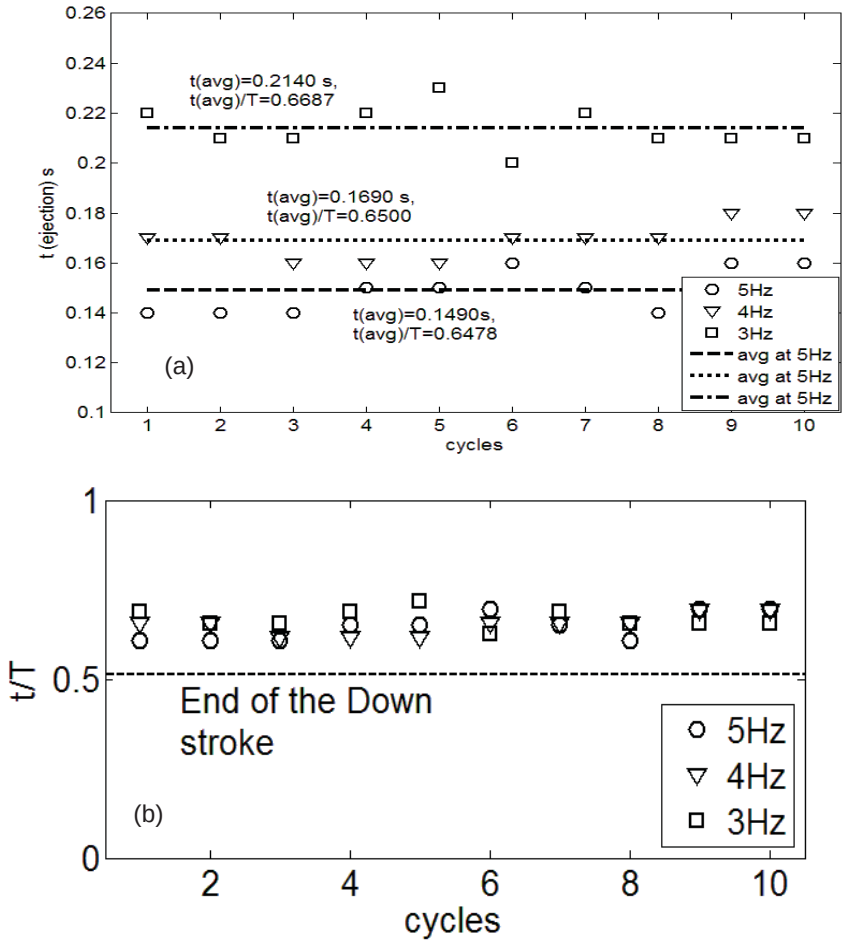

Fig 4.10 (a)Ejection timing at different frequencies for 1.75X wing (b) nondimentional timing of the ejection

Similar patterns are also seen for 1X wing mounted on the same model 1.

The experiments are also conducted on model 3 with lead lag motion. The nature of LEV TEV growth is similar to the one shown. However there is a little difference in the smoothness of the flow involved with the lead lag motion. The flow is more regular smooth and the vortices are better attached to the wing surfaces with less breaking up into parts. The sequence of PIV for model 3 is shown in Fig 4.11.

In Fig 4.11 the PIV results are shown as velocity vectors superimposed on vorticity contours. The levels of the contours as shown in the legend are scaled by a factor of thousands. So a value of 0.2 would mean 200 as the actual vorticity level. Blue contour shows clockwise rotation and red and yellow shows anticlockwise. The white line shows the location of the wing with the white dot showing the leading edge.

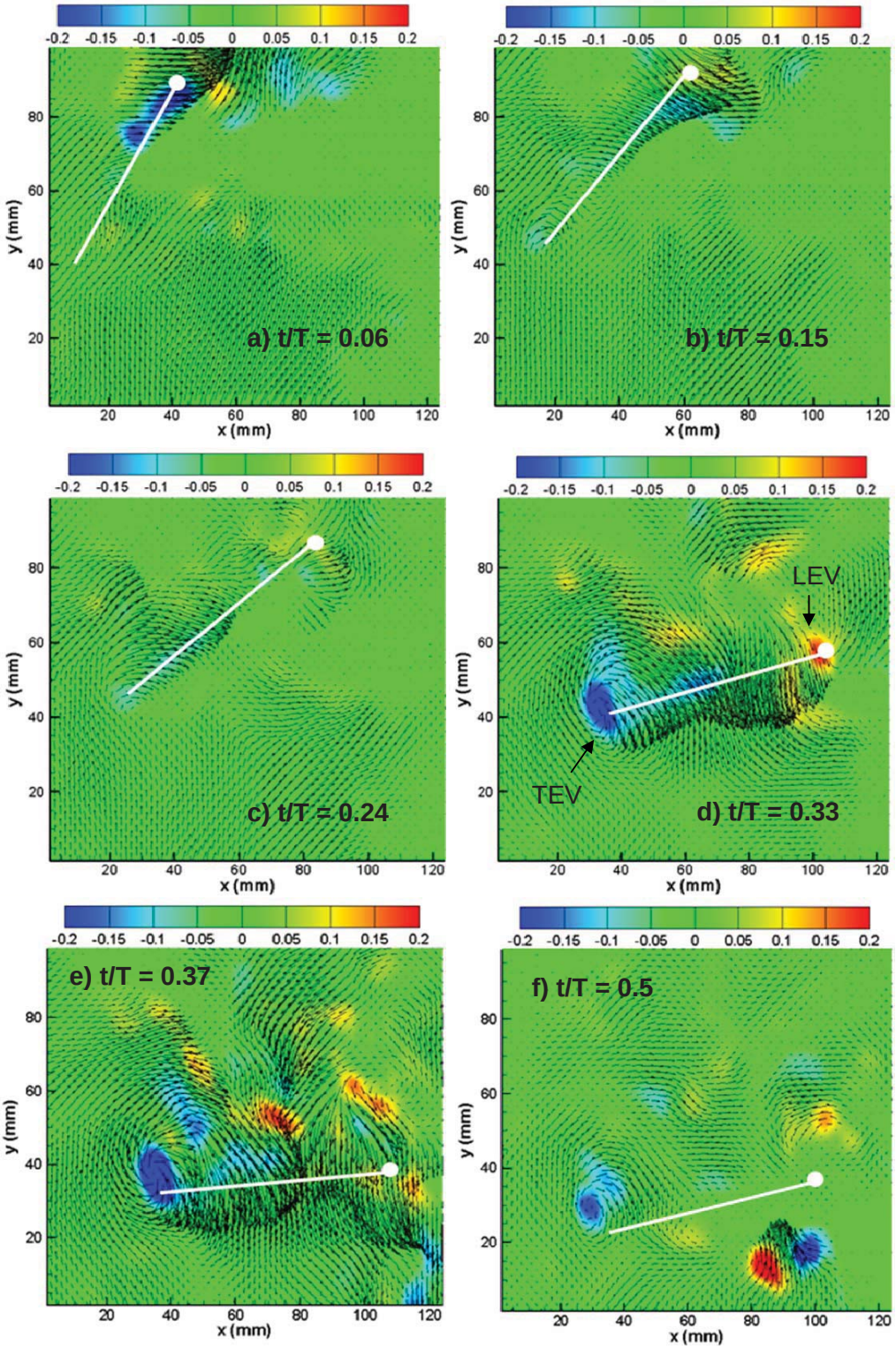

Fig 4.11a-f Downstroke for model 3 at 0.5 R span length at 5Hz, Re =2830

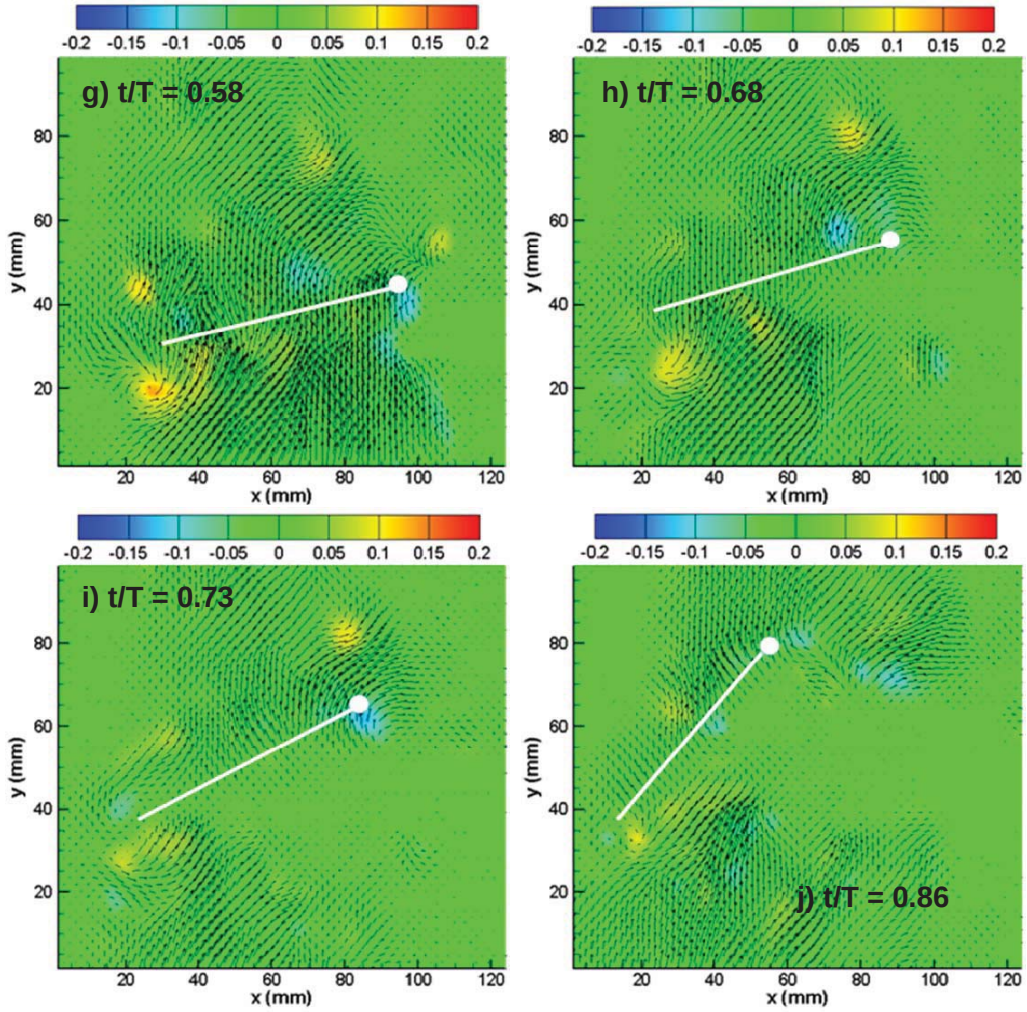

Fig 4.11g-j Upstroke for model 3 at 0.5 R span length at 5Hz, Re =2830

As can be seen from the series of 4.11 the vortex LEV and TEV are better attached. As the laser sheet is falling from left to right there is a little shadow below the wing in some pictures depending on the orientation of wing. As TEV is viewed better we are interpreting the LEV as well through our observation of TEV as the kelvins theory of circulation holds.

The circulation of the vortex resulting in lift generation have been evaluated and plotted in Fig 4.12. it can be seen that the effective circulation is more in the downstroke than in upstroke leading to net lift production. The sudden and sharp fall in circulation during the stroke reversals from downstroke to upstroke (after t/T=0.5) shows the intense interaction of the vortex pairs formed during this time. Though there is no ejection visualized as such as the Re number and the wing translational velocities are low, but there is subsequent sustaining of a part of the TEV as seen in Fig 4.11 (i).

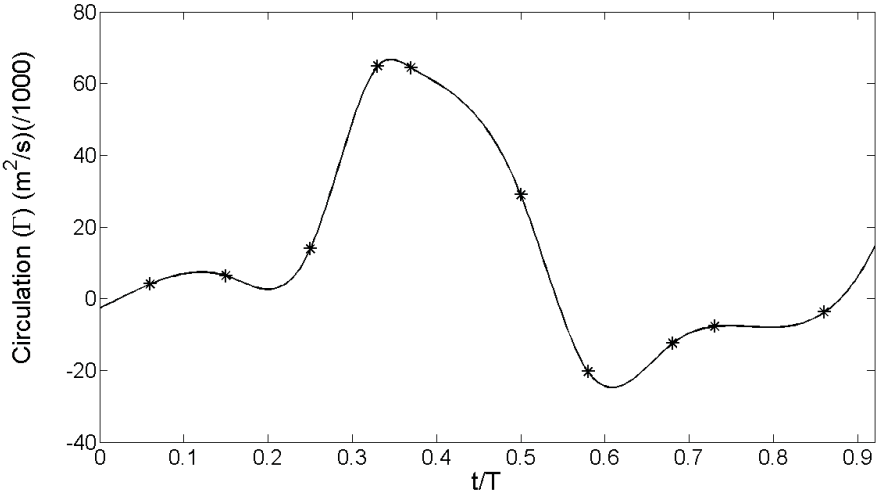

Fig 4.12 Circulation variation of LEV with flapping cycle. (t/T=0 shows start of downstoke)

Similarly the size of the forming TEV with the downstroke has been shown in Fig 4.13. It can be observed that just like circulation the size is maximum around t/T=0.37 and it falls towards the end of downstroke.

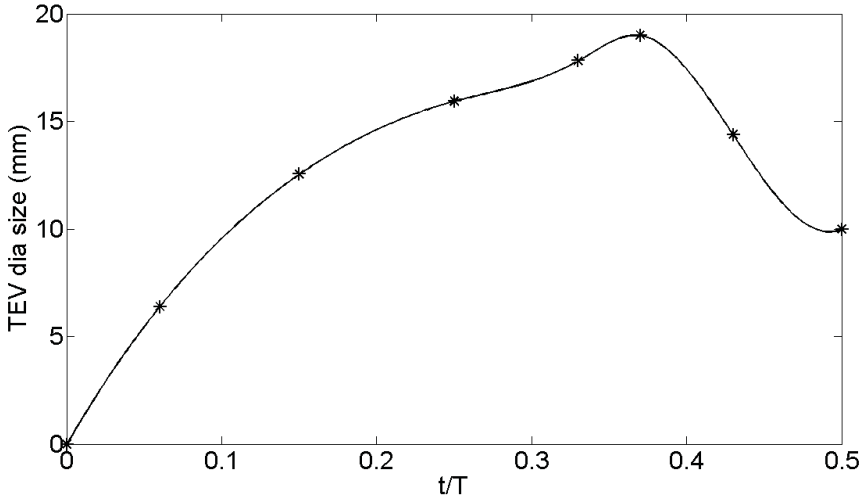

Fig 4.13 Size variation of TEV along downstroke (t/T=0 shows start of downstoke)

Similar conclusions can also be drawn by the variation of maximum vorticity of TEV with downstroke (Fig 4.14).

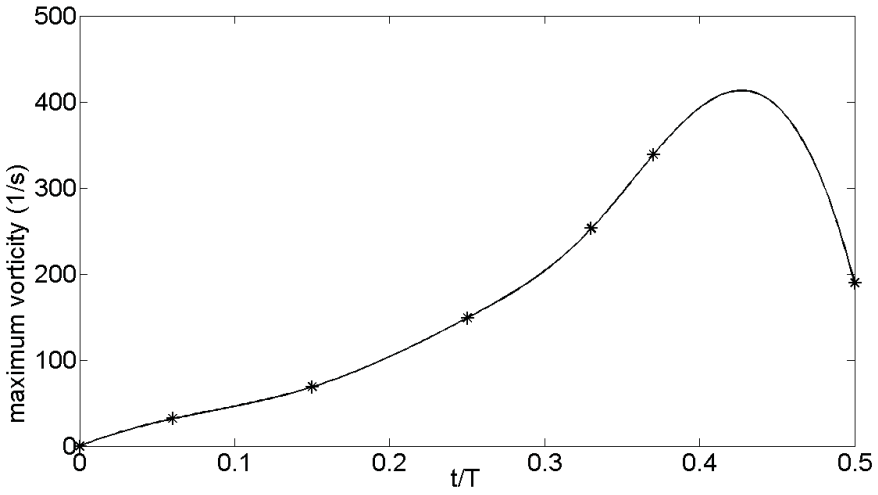

Fig 4.14 maximum vorticity variation of TEV along downstroke (t/T=0 shows start of downstoke)

Apart from the force calculated from the load cells, forces are also calculated from PIV results (Fig 4.15). As PIV gives velocity data in a plane, knowing the position of the wing momentum analysis can be done easily in a control surface surrounding the wings. This will give the forces in that particular plane. By taking 2D (two dimensional) assumptions forces over the wing are estimated. Though this will be a rough estimate as the actual flowfield is highly 3D (three dimensional), but here, as we are interested in the pattern and nature of the force, this rough estimate will even benefit our understanding of the flow physics over such flapping flight. As there is no forward velocity the thrust generated can be given as

Thrust (N) = ρAU^2 …….…… (eq 3)

Where ρ is the density of air (1.225kg/m^3), A is the frontal area (wing span*thickness), U is the root mean square velocity in the wake profile.

Thus the thrust variation along a cycle is calculated through the data extracted from PIV results on model 1 for both 1.75X and 1X, and are plotted in Fig 4.15. As per the assumption the cycle starts with downstroke thus till 0.56t/T on the time scale is downstroke and the rest is upstroke. Thus during the ejection at this point a significant thrust is expected and it is verified.

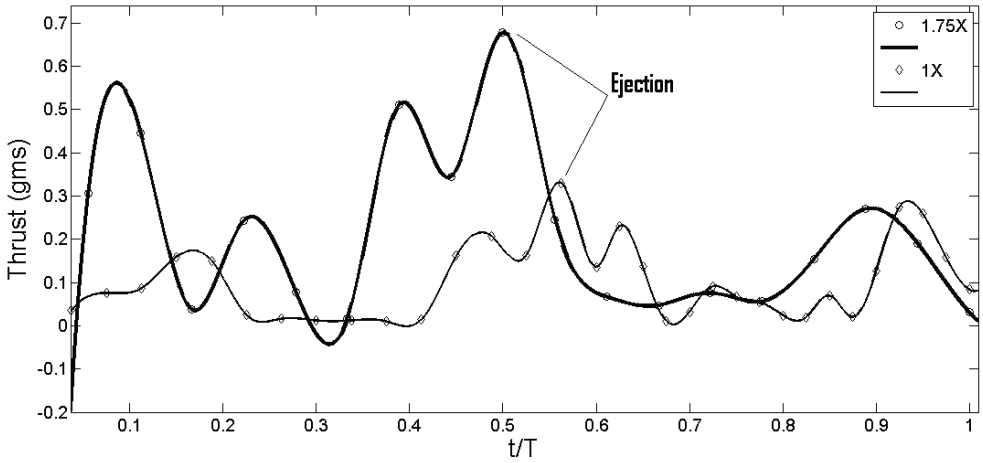

Figure 4.15 variations along time for model 1 using PIV data

As predicted in the PIV results that the time of shedding is delayed for the 1X wing due to its lower feathering angle as well as due to the staying of the TEV a little longer than 1.75X, the same can be seen from the Fig 4.15 where the thrust maxima for 1X model is delayed than the 1.75 X model. Here it is well seen that the total and average thrust is more with the increase in the size of the wing. Thus the PIV results are in perfect agreement with the load cell data.

The model 2 with forced feathering is not put directly onto the load cell. But yet the force estimation of the thrust is done using the PIV data momentum analysis as discussed for model 1. The thrust variation looks very smooth and the effect of shedding at both the stroke reversal points is well observed. The nature of the thrust generation is also similar (Fig 4.16 a). Wheras for model 3 (Fig 4.16 b) it can be seen that thrust generation is different in the sense that it is mostly negative till a little ahead of mid of downstroke and then remains fairly positive. The negative part of the thrust can be explained from the higher angle of the wing creating a component in the drag direction making the thrust negative.

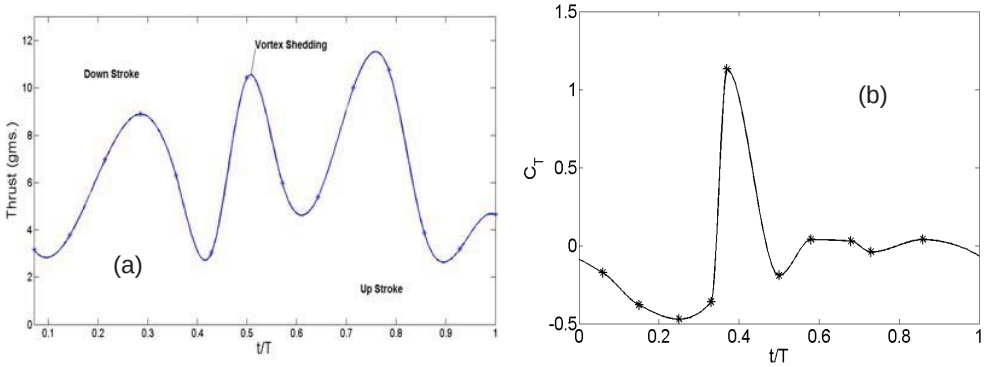

Figure 4.16 (a)Thrust Vs t/T (For Model 2) (b) Thrust Vs t/T (For Model 3)

3D results

The setup for conducting the experiments to measure 3D flowfield is similar except that instead of one, two cameras are set and caliberated in a stereoscopic view as shown in Fig4.17 (a). The measurements are done at 10locations as shown in Fig 4.17(b).

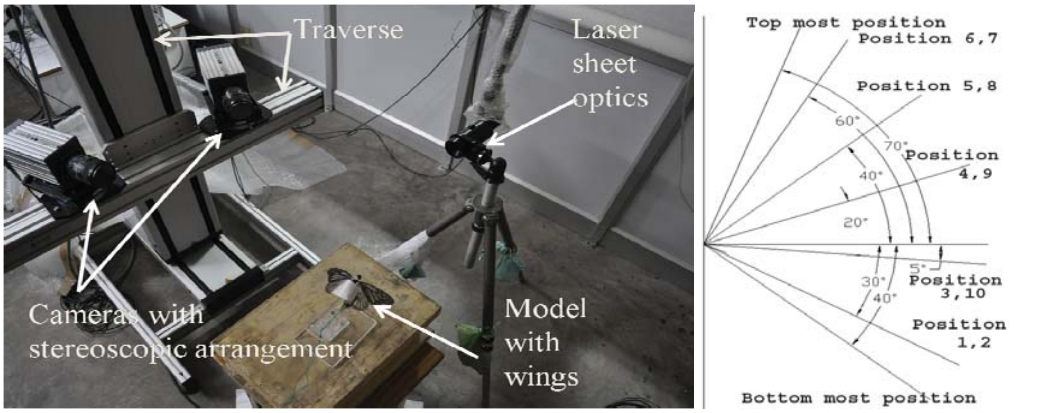

Fig 4.17 (a)stereoscopic arrangement for the 3D experiments (b) 10 locations of measurement.

Measured velocity and vorticity field at different positions (marked in Fig 4.16b) are shown in Fig 4.18-4.24. In these figures the velocity in the plane of measurement is shown as vector arrow and the background contour in (a) is vorticity and that in (b) is spanwise, 3-rd component of velocity. In (b) (in (c)) the blue and red levels show respectively, clockwise rotation (spanwise w velocity into the plane of paper, indicate spanwise velocity towards the root) and anticlockwise rotation (w velocity out of the plane of paper, indicate spanwise velocity towards the tip). The wake profiles in the vicinity of the trailing edge are shown in (c). The flapping cycle is assumed to be starting with downstroke, thus t/T=0 denotes the starting of the downstroke. The position of the wing is also shown by a straight white line. Here only a little of the trailing edge of the wing is captured. The beginning of downstroke for flapping frequency 5Hz (Re=10080) has been shown in Fig 4.18 at t/T=0.05. The downstream velocity far above the wing is the clapping effect of the previous upstroke. The vortex with anticlockwise circulation, under the wing, which is produced during upstroke remains attached at this time (beginning of downstroke). As the wing moves downwards the vortex below it as well as the effect of clapping (as can be seen by the stream of air leaving at the upward side) diffuses gradually. The spanwise component of velocity, w (contours of Fig 4.18b) at location 0.5R shows considerable spanwise velocity towards the tip. Velocity profiles (U component) at four x locations of the wake near trailing edge are also shown in Fig 4.18c to put light on the nature of flow leaving the trailing edge. These wake profiles aids in our understanding of the captured vortical structures near the wing or any other phenomenon like vortex pair ejection due to the mutual interaction of the vortex present in the wake. During clapping, trailing edge lags behind the leading edge due to wing flexibility, which results a thrust producing jet downstream as seen in Fig 4.26 and 4.18. In this

configuration, at the wake of the wing, if the mean of Uavg at the trailing edge is negative, the thrust is positive. Though the actual flow is three dimensional and complex but the nature of distribution of this Uavg at the trailing edge at any chord cross sectional plane provides an idea of the nature of variation of thrust generated. The estimate of thrust from this data has been made using the 2D assumptions only as discussed earlier.

At time t/T=0.15 the wing moves a little down as shown in Fig 4.19. The decreased levels of vorticity show the weaking or the decay of the vortex below the wing that has been formed in the upstroke. No vortex formation above the wing surface is observed at this time. Though the effect of clapping is still visible (Fig 4.19a) but the values are much less than the previous time, t/T=0.05. The spanwise flow is present over and below the wing due to 3D nature of the flow. The reduced values of Uavg (Fig 4.19c) imply loss of thrust at this time.

As the wing moves further down, the effect of trailing edge deflection and fling effect brings a jet of fluid above the wing as seen in Fig 4.2a-c at t/T=0.25. The vortex below the wing as seen so far in the downstroke has now vanished or totally decayed. A strong spanwise flow over the wing indicates that this jet leaves the trailing edge at an angle resulting increase in thrust. This can also be seen in Fig 4.26 at t/T =0.25. Circulation above and below the wing at this time is nearly zero indicating a less or negative lift at this time. As the wing moves further down, a TEV develops over the wing. The Fig 4.21 shows the flow fields at t/T=0.34. This TEV (which simulates the LEV in this case) which is clockwise and shown by blue levels of vorticity is responsible for most of the lift generated as recognized in past studies. The major target of the researchers is to make this LEV or TEV stay for longer time so as to optimize the lift. But a lot depends on the wing kinematics and morphology and thus possess a tough challenge to unreveal. The control over this growth and stability of the LEV or TEV would bring a lot of progress in this flapping field. But the unsteady nature and the variation with Re and from species to species in natural fliers makes it difficult to generalize.

With the progress in downstroke, the wing instantaneous velocity increases and reaches to its maximum along the midpath. Due to the high instantaneous velocity of the wing periphery shear layers are fed into the TEV making it grow in strength and size. At t/T=0.34 a clear and distinct TEV is observed (Fig 4.21a). Spanwise flow develops towards tip below the wing and towards root above the wing. This spanwise flow is combined effect of three dimensional TEV due to the backward sweep of the wing, spanwise flow generated due to clap and fling effect and angle of measurement plane and TEV axis. With the instantaneous flapping velocity maximum the TEV grows and the thrust contribution in this stroke attains a peak value (Fig4.21c, Fig 4.26). This can be reasoned by the fact that with flexible Mylar membrane wing, it deforms chordwise and bends more at this location leading to an induced angle to attack to the flapping velocity and owing to the contribution of the TEV the thrust generation is higher.

As the stroke reaches its end t/T=0.48 (Fig 4.22a), the shear layer still continues to feed into the TEV making its unstable and grow in size and vorticity levels. Thus the TEV structure doesn't remain fully intact like before anymore. Rather it breaks or segments into a few vortex which detaches from the primary TEV and there is a stretch of TEV segments along the whole trailing edge profile over the wing (Fig 4.22a). The profile plots of velocity near wake show a decline in the thrust production. This can be contributed to the reasoning that due to the fragmented portions of TEV it imparts

positive Uavg above the wing at certain points. As the stroke changes from downstroke to upstroke, the TEV which is already at higher vorticity levels doesn't just decay instantaneously. With the change in flapping direction or the retardation of the wing towards the end of the downstroke another vortex of opposite nature and circulation of TEV starts forming just below the wing. The pair of vortices starts mutually interacting by inducing velocity on each other and in the region between them. The velocity imparted to the fluid in between them adds up and it gushes through carrying away most of these vortices along the wake. The newly formed vortex below the wing has a high circulation value owing to the maximum angular acceleration of the flexible wing at the start of the upstroke. High momentum of air leaving the wing imparts a reaction force to the wing, which resolves into considerable lift and thrust depending upon the direction of the imparted velocities. This sudden and rapid interaction of the vortex pair leading to high lift and thrust is referred to as the Ejection phenomenon. Depending upon the orientation of wing at this stroke, the Re range and the geometric location of the formed vortices in the form of a ring which further depends upon the contour of the wing, the contribution of this ejection can be studied. Momentarily the thrust forces can be identified by the higher magnitude of Uavg leaving the wing at the stroke reversal. That's what is performed here, by looking into the velocity fields of the PIV data (Fig 4.23a). One more thing worth observing at this point is that this ejection direction in this case of butterfly resembling wing at 0.5R is not just in the chordwise direction, also has got some spanwise component present in it (Fig 4.23b). This conveys that the ejection of the vortex rings as a structure or as fragments acts in a direction outward in some sweep direction leading to its components both in chordwise and spanwise directions. These interacting vortex rings might perhaps explain the concept of formation fight in birds where they fly behind each other at an angle and by a fixed flight distance. Though the exact nature and dissipation of energy of these ejected ring structures have not been studied yet but this ejection phenomenon does open up a lot of other interesting observations particularly during maneuvering. This ejected pair of vortex passes along the wake with the progress of upstroke. We find that the effect of it is still felt in the preceding position of the wing (Fig 4.24c). With the upstroke continuing the vortex below the wing develops and grows (Fig 4.24a). This is the point where the circulation is totally negative and negative lift follows. The wing is near the middle of the upstroke and has maximum upward velocity. This high flapping velocity is responsible for the higher thrust (Fig 4.26). Similarly the spanwise flow also develops over and below the wing in a direction opposite to the case in downstroke, outwards over it and inwards below it (Fig 4.24b)

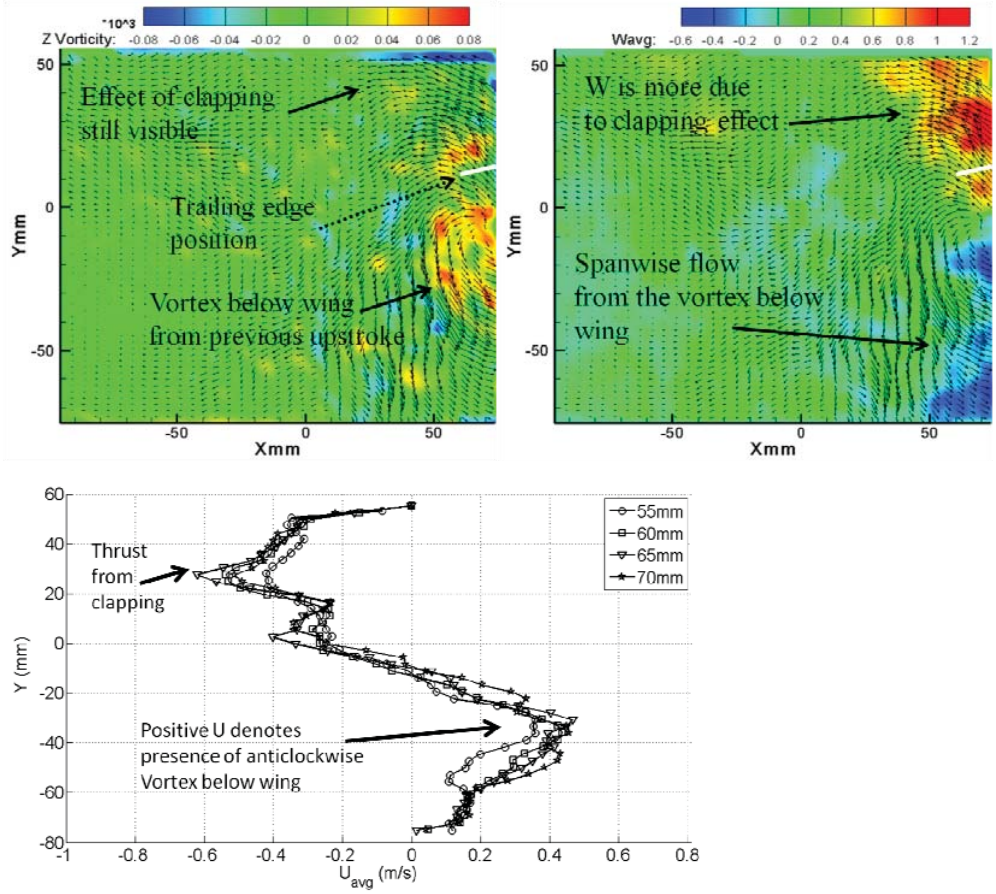

Fig 4.18 Velocity field at beginning of donwstroke, t/T=0.05. (a) U and V components superimposed on vorticity contours (b) U & V superimposed on W (c) plot of Uavg at the wake near trailing edge.

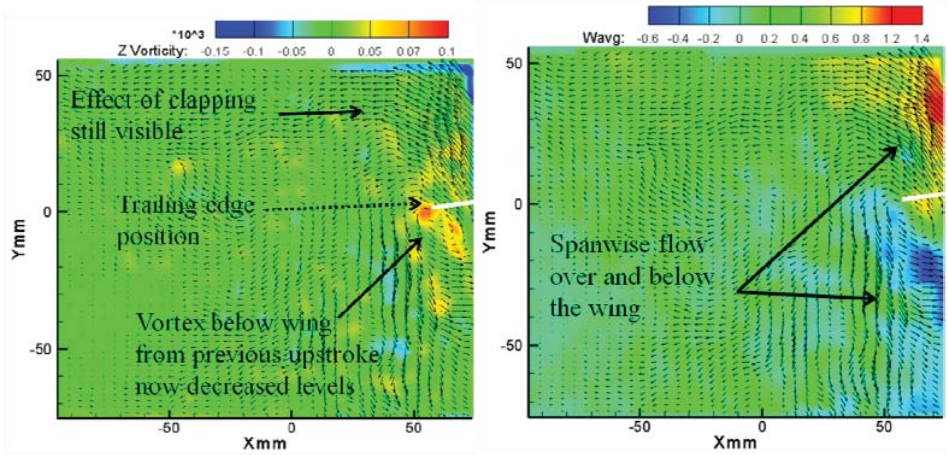

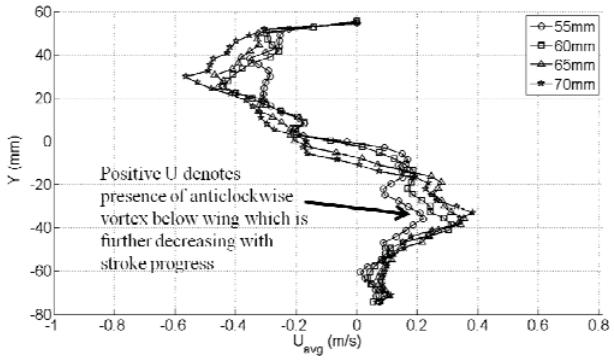

Fig 4.19 Same as Fig 4.18 at t/T=0.15. Mean value of Uavg decreases than the previous measurement showing a considerable drop in thrust.

From Fig 4.18-4.24, the growth of TEV whose nature replicates the LEV in our case can be easily visualized from the levels of vorticity as well as from the size of the vortex. The TEV breaks down into segments towards the end of the stroke and doesn't remain very intact in nature as one structure due to the feeding of shear layer vortices along the periphery of the wing. During the downstroke at 0.5R it can be clearly seen that there is always a spanwise flow shown by the W_{avg} which verifies that the vortex is of 3D nature and rolls up normal to the wing surface a component of which shows in the W_{avg}.

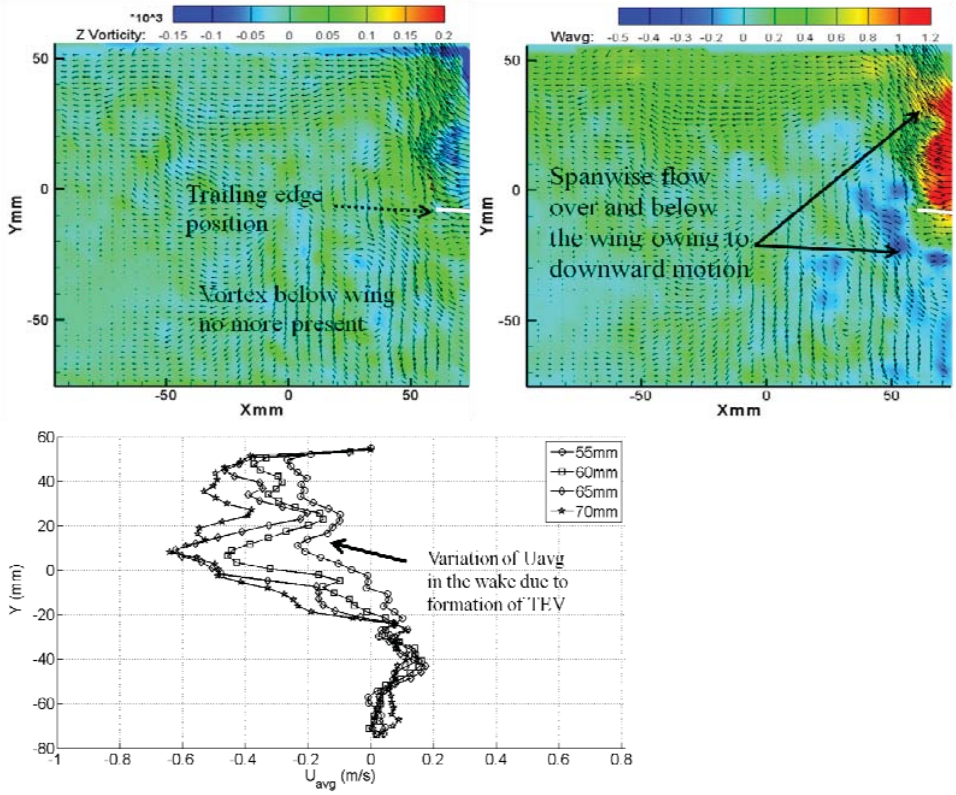

Fig 4.2 Same as Fig 4.18 at t/T=0.25. Mean value of U avg being negative shows a rise in thrust than the previous location

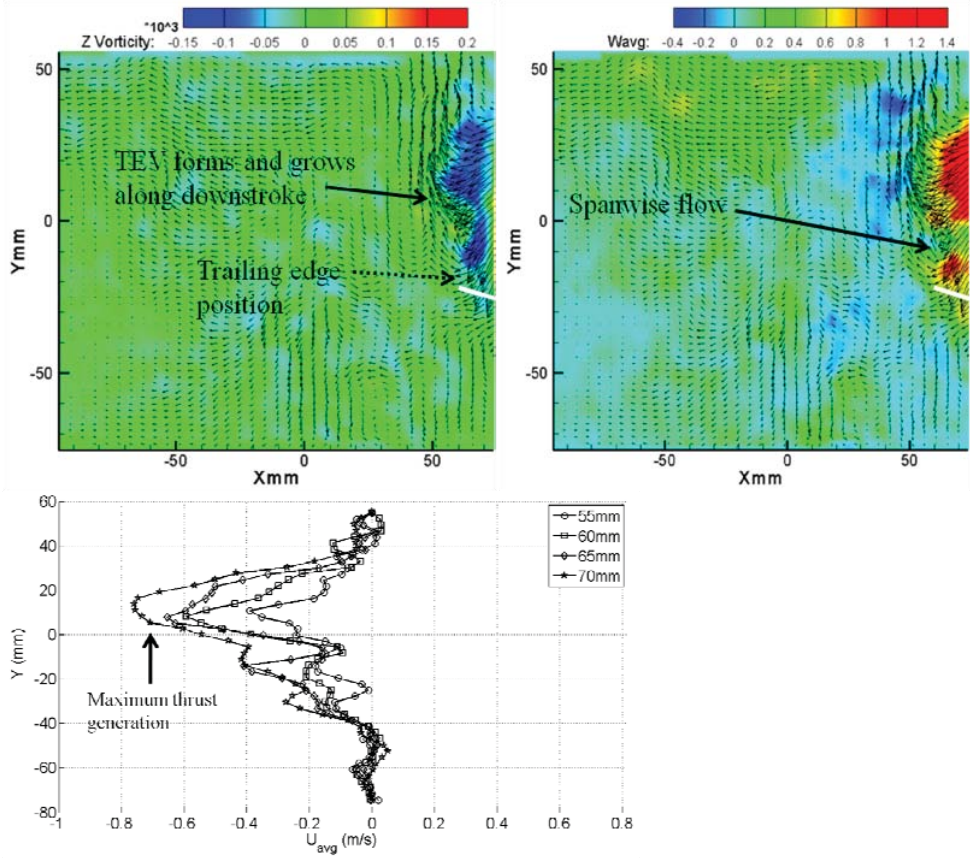

Fig 4.21 Same as Fig 4.18 at t/T=0.34.TEV grows in size and strength as seen from the vorticity levels. All values of Uavg are negative showing a further rise in thrust generation reaching its peak in the downstroke.

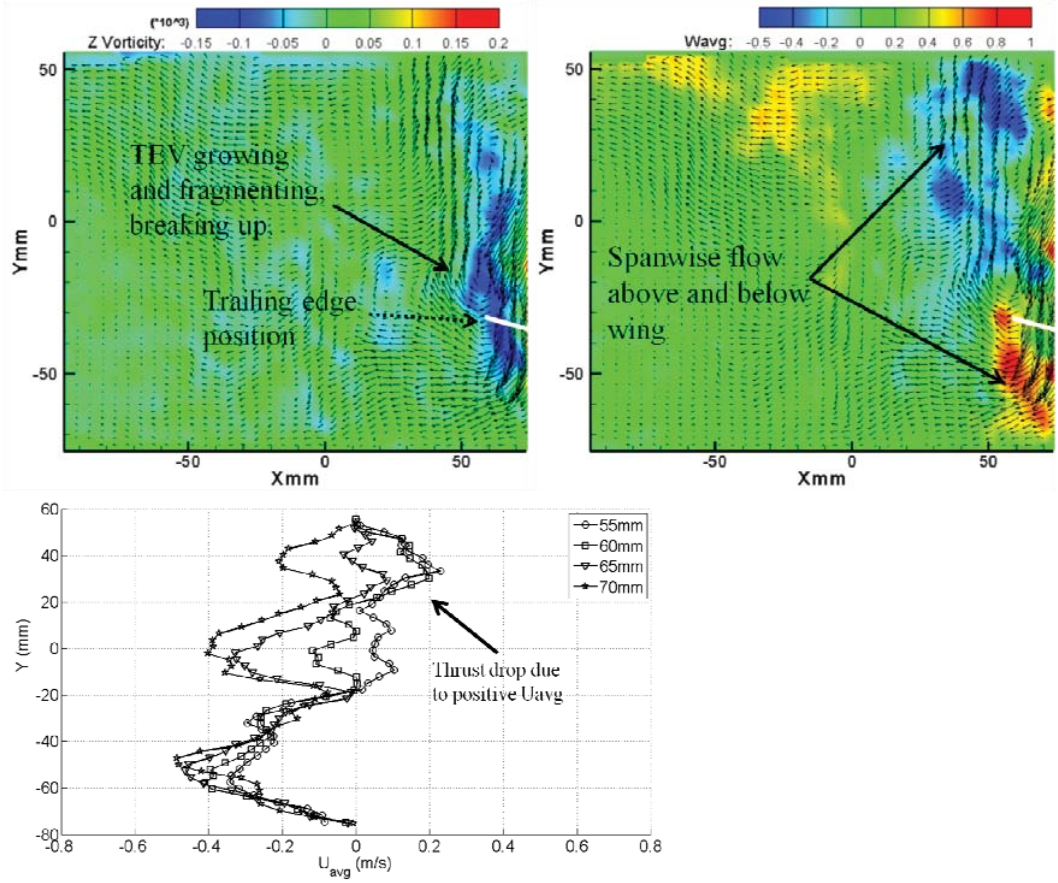

Fig 4.22 Same as Fig 4.18 at t/T=0.48. More positive figures of Uavg show a fall in thrust generation. The TEV becomes unstable through the continous feeding of shear layers and owing to spanwise flow it breaks down into components thus vorticity levels stretching all over the near wake region.

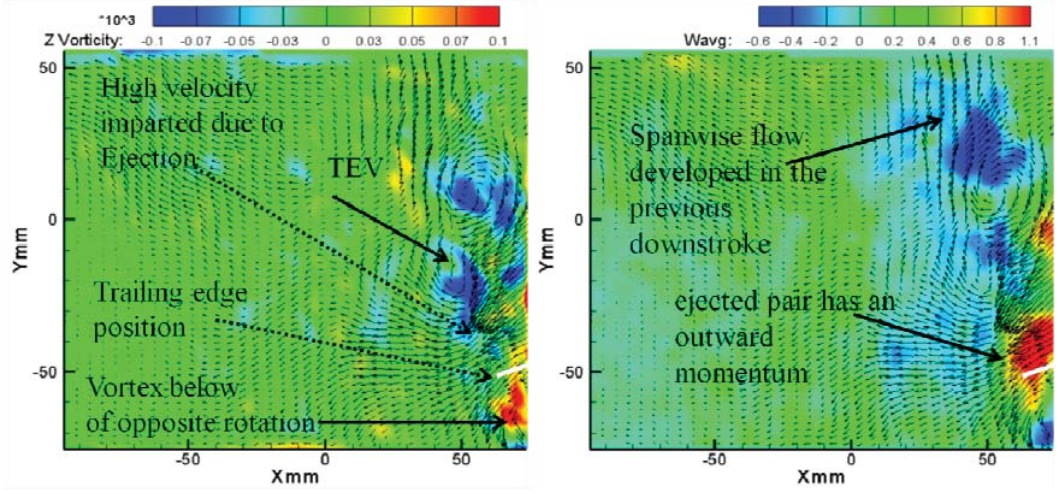

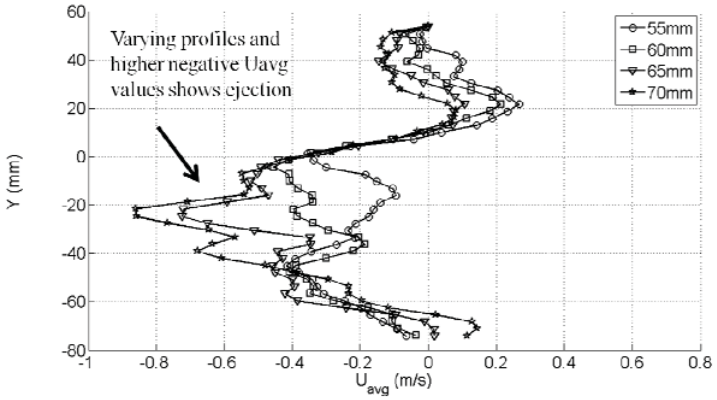

Fig 4.23 Velocity field at beginning of upstroke, t/T=0.6. (a)The vector field shows U and V components superimposed on vorticity contours (b) Velocity field superimposed on the spanwise W component of the averaged velocity (c) plot of Uavg at the wake near trailing edge. The ejection of the pair is observed leading to high thrust at the stroke reversal.

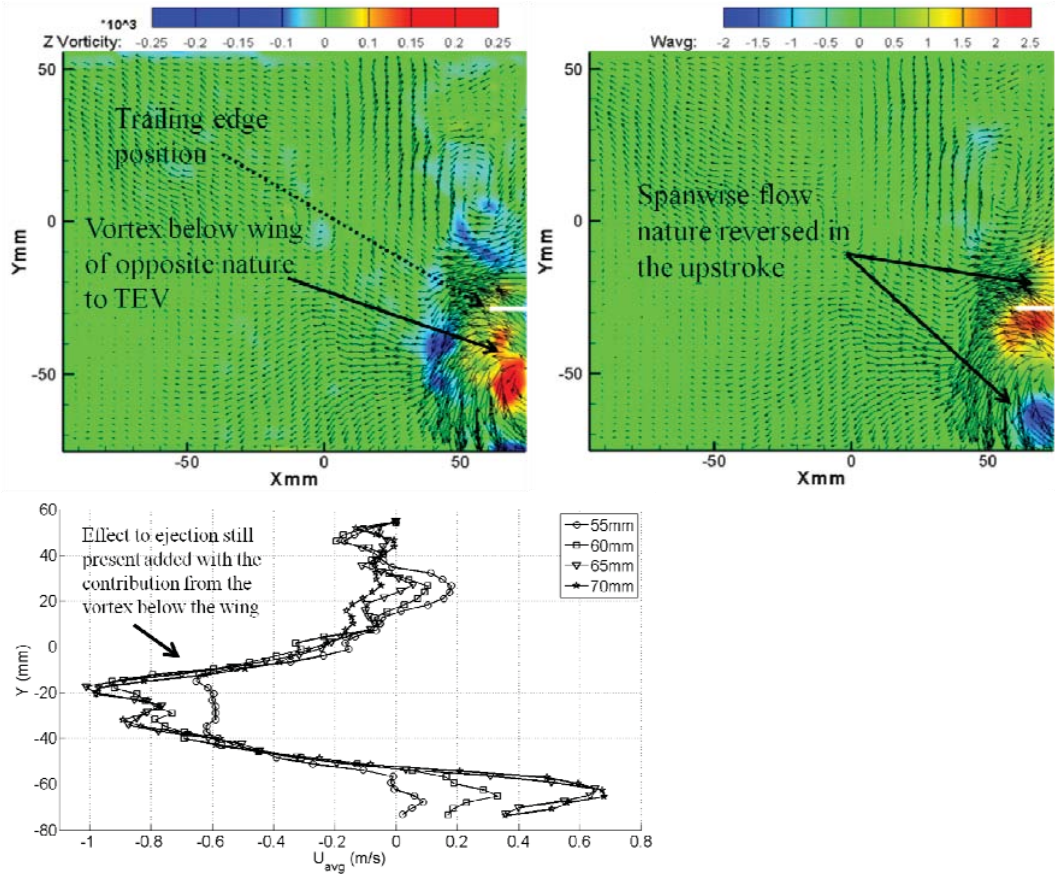

Fig 4.24 at t/T=0.7. (a)The vector field shows U and V components superimposed on vorticity contours (b) Velocity field superimposed on the spanwise W component of the averaged velocity (c) plot of Uavg at the wake near trailing edge.

The circulation is calculated from the wake velocity field at the near vicinity of the trailing edge up to three quarter chord lengths. The circulation at the measured locations of the flapping cycle is shown in Fig 4.25. The circulation distribution in turn gives the insight of the nature of lift forces encountered and puts light even to the cases in presence of forward velocity (circulation contribution in the flapping). The vortex above and below the trailing edge of the wing are captured with their corresponding contributions in the net circulation. The sudden change in circulation or the sudden shift in the values changing its sign at the stroke reversal shows the ejection of the TEV pair and its corresponding contribution to lift or thrust in Fig 4.25-4.26.

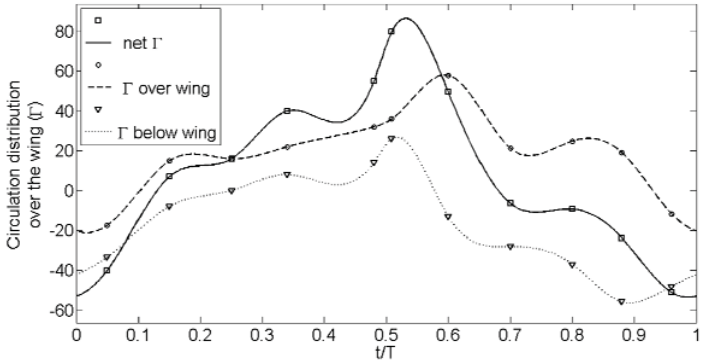

Fig 4.25 (a)Variation of circulation with time at 5Hz

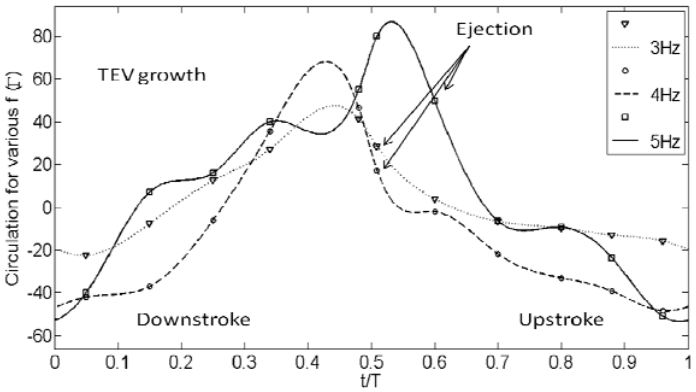

Fig 4.25 (b) Variation of circulation with time at various frequencies

Again thrust values are calculated using the similar way as already discussed in the 2D section, but this time the calculations are done at the mentioned 10 locations and fitted with an interpolant spline curve. The effect of ejection and clapping is clearly visible. The thrust generation remains all positive for the total cycle.

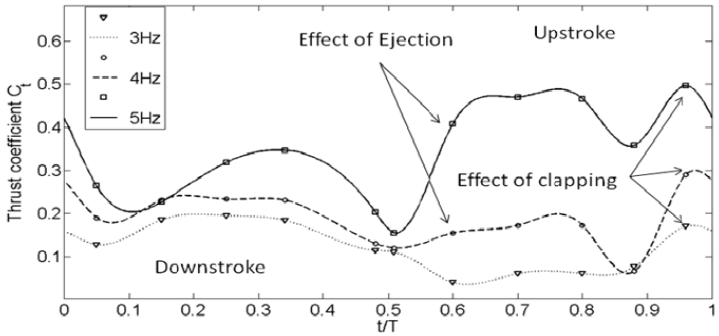

Fig 4.26 Thrust variation with the flapping cycle from experimental evaluation

5. Discussions

5.1 Force

If the force results are compared for model 1 and 3, certain significant observations can be made. First of all by looking into the FFT of the raw data of force experiments it can be seen that there are a number of harmonics for the model 1 cases whereas the flow is much clear in case of model 3 with the same wing (Fig 5). The same can also be reasoned through the PIV results that the vortex are more attached in case of model 3, and not breaking up into parts in case of model 1, possibly giving rise to those many harmonics in the latter case.

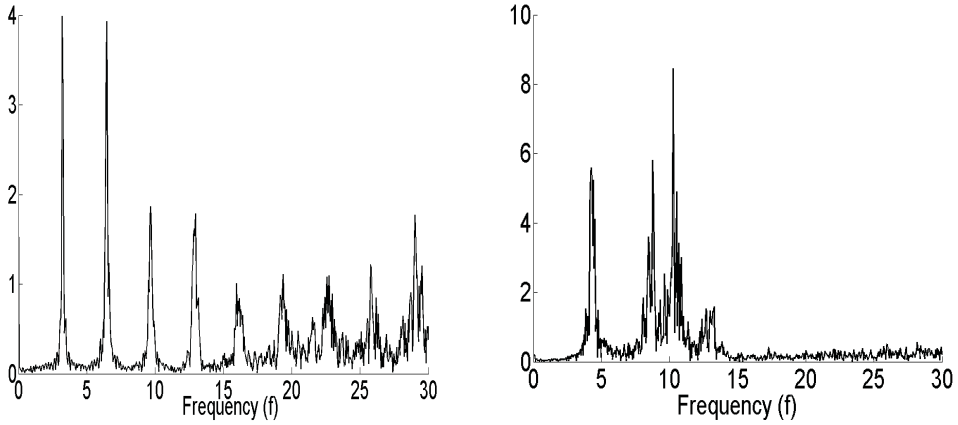

Fig 5.1 (a)Lift raw fft of 1.75X wing at 3.2Hz for model 1, Re =4008 (b) Lift raw fft of 1.75X wing at 4.2 Hz for model 3, Re=1583

Again it can be seen through force results that for both the models lift and thrust vary inversely with J. The same trends was also observed in the earlier experimentsand study performed in the masters thesis of Mr. Abhijit banjerjee (Fig 5.2a).The rotational component of thrust also falls with flapping frequency for both the models. Whereas the rotational component of lift increases with frequency upto a certain point and then falls

again for model 3 the same may explain the attaining of maximum lift at a certain frequency. For model 1 the rotational component of lift more or less remains the same and rather decreases very gradually which is more a parameter of the kind of wing.

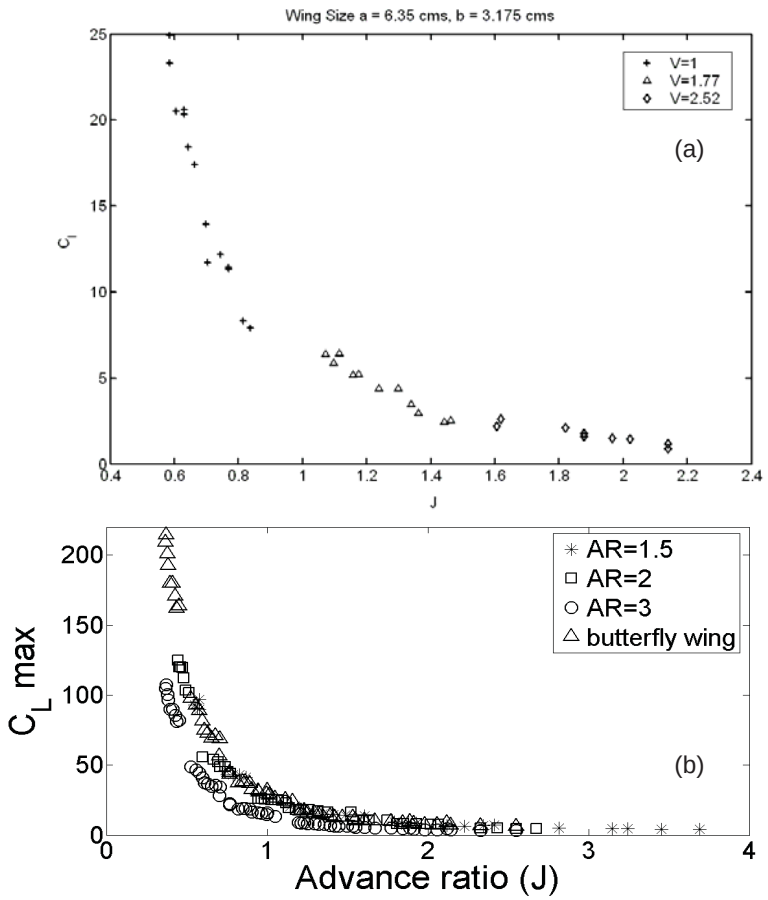

Fig 5.2 (a) C_L vs J for wing size (a=6.35 cms, b=3.175 cms) (earlier study)
(b)C_L vs J for wing size for various wings tested on model 1 (new study)(already shown in Fig 3.12)

5.2 PIV

As already discussed in the PIV results the nature of flow is similar for all the models as all of them are vortex dominated flows in the unsteady regime of zero forward velocities. The basic phenomenon of formation and growth of LEV and TEV are more or less similar in all the cases except for certain timing and strength which is more a parameter of the involved Re and wing kinematics. However there are certain obsevations worth mentioning. While comparing the PIV sequence of model 1 (Fig 4.1-4.7) and model 3 (Fig 4.11) it is clear that the flow and the vortex are much attached to the wing for model

3. The same can be properly shown by picking 2 pitures of both cases at the same time ratio of the flapping cycle.

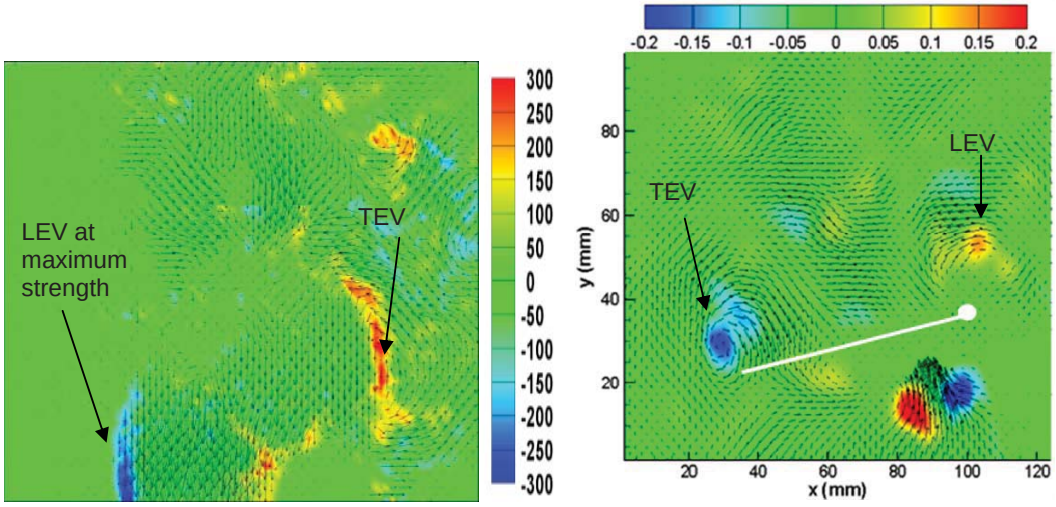

Fig 5.2 PIV results of model 1 and model 3 respectively at t/T =0.5

As can be seen from Fig 5.2 that the vortex are much stretched and elongated and broken into parts for model 1 case, whereas the vortex for model 3 case are much intact and attached to the corresponding sufaces.

By looking into maximum vorticity of these 2 cases it is found out that for model 1 the maximum vorticity is during the end of the downstroke (Fig 4.8) whereas for model 3 (Fig 4.14) the maximum vorticity is a little away from the mid of the downstroke. The same conclusion can also be made out for the vortex sizes as well as the circulation scnearios. Apart from this the circulation variations for these two models depict a significant conclusion. For model 1 the circulation in both the strokes are quite similar in nature and magnitutude the downstroke being greater in magnitude with the maxima at t/T =0.5. For model 3 the circulation of the downstroke is much higher in magnitude than that of upstroke verifying that fact that lift coeffcients of model 3 are much higher. Again the maximum circulation of model 3 is near t/T =0.4.

5.3 Wing size, shape and flexibility

From the experiments and results so far it has been quite mentioned that for a particular given kinematics of the wing the lift and thrust forces will depend on the Re number, the frequency, the span size of the wing, shape, flexibility etc.

The flapping frequency and the span size of the wing have a direct impact on the force generated by being directly proportional to the Re number (eq1). Whereas the shape and flexibility has indirect and significant effect by changing the nature and timings of important phenomena involved in the flow.

From the force results on model 1 with varying J values it can be observed that the butterfly wing of 1.75X has better coefficients of both lift and thrust in comparison to a rectangular wing of the same AR and span (Fig3.11-3.16). The possible reason being the LEV or the whole vortex ring that extends over the periphery of the wing is more stable and strong with respect to the rectangular wing of similar material, AR and span. This is the effect of the wing shape which can be later studied into details. The same can also be seen by comparing the lift forces with t/T of both the rectangular wing and the butterlfy wing. (Fig 5.3). it can be seen that the downstroke for 1.75 X wing produces more positive lift and the upstroke less negative lift than the rectangular wing of AR=2.

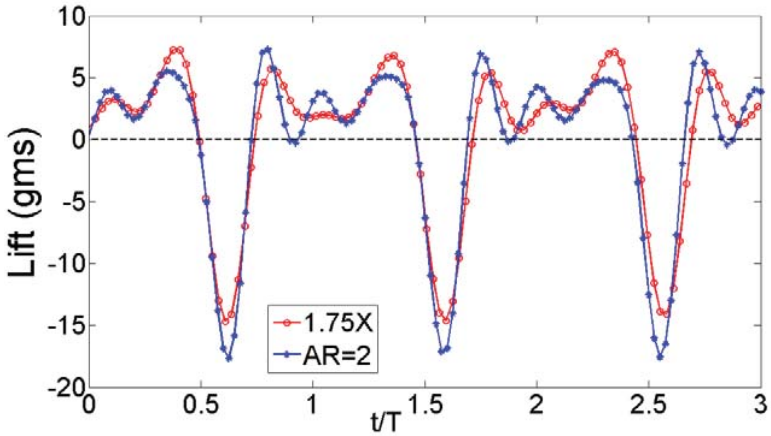

Fig 5.3 Comparison of lift for butterfly and rectangular wings at 2.9 Hz showing the importance of shape.

Flexibility is another important criterion when it comes to optimum lift and thrust forces. The same has been studied by testing 3 rectangular wings of same span length and different chord lengths or different aspect ratios (AR) on model 1. As chord length increases or the AR decreases the wing gets less rigid (as only the leading edge of the wing is fixed to the model). The chord being longer and further free to deform in the chordwise direction provides the chordwise flexibility to the wing. From the Figures 3.11-3.16 it has been seen that the rectangular wing with AR=2 gives better result among other rectangular wings. The reason is that it has the optimum flexibility among the other rectangular wings. The little rigidity it has more than AR=1.5 wing makes it produce better lift whereas the little flexibility it posseses over the AR=3 wing makes it generate better thrust forces as well. This is just the initial verification of the importance of flexibility and the study has only been done in the chordise region. A much detailed study can be later conducted with both spanwise and chordwise flexibility coming into play and choosing a better optimum wing in that case.

5.4 Optimum wing and optimum model

Wing kinematics is a critical factor in the behaviour and nature of the forces produced. Given a particular model with a particular degree of freedom the kinematics is fixed. However the shape and size of the wing and its flexibility also plays a role in defining the

kinematics of the overall motion. The same is studied by using various models and various wings.

In this particular study, the model represents the degree of freedom alloted to the wing structure. Moreover depending upon the size shape and flexibility of the wing material additional degrees are introduced due to deformation in a particular fashion.

In model 1 and model 3 the differnce in the general kinematics is studied by incorporating additional degrees of freedom in the linkages. Model 1 only undergoes flapping while model 3 undergoes a combination of flapping feathering as well as lead lag motion. Though the combination of the three is not controlled or coordinated in any known fashion. But the motive of studying the underlying effect of wing kinematics by incorporating freedom in the linkages is well achieved.

Again for the same model 1 a variety of wing shapes and sizes are used to study the dynamics and force nature of varying wing shapes sizes and flexibilty.

While using 3 rectangular wings of different cross section and butterfly wings, all of the same span, the longitudinal flexibility is constrained or made similar, whereas the focus is shifted to the shape and chordwise flexibility only. The results of force study off all of them can be summarized into Fig 5.4-5.6

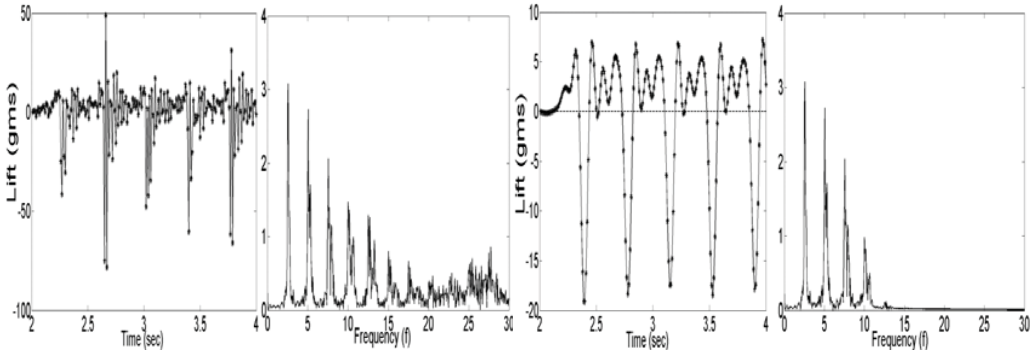

Fig 5.4 (a)raw lift data(b)fft of (a) (c) filtered lift data (d) fft of (c) for AR=2 rectangular wing at Re=4587 at flapping frequency 2.9Hz on model 1

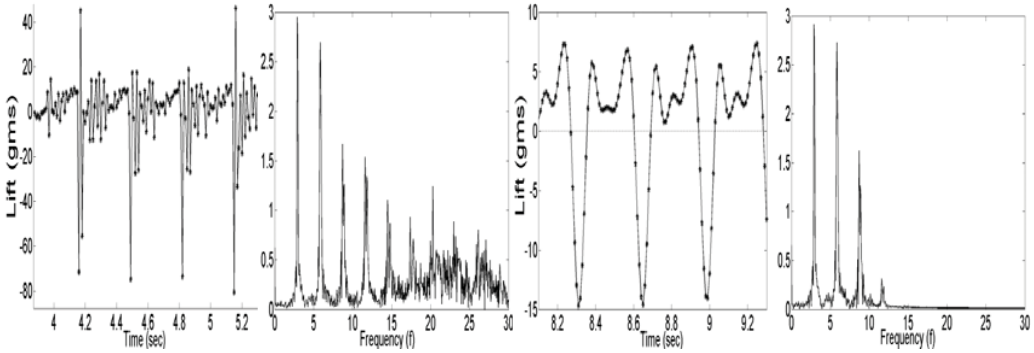

Fig 5.5 (a)raw lift data(b)fft of (a) (c) filtered lift data (d) fft of (c) for 1.75X butterfly wing at Re=4008 at flapping frequency 2.9Hz on model 1

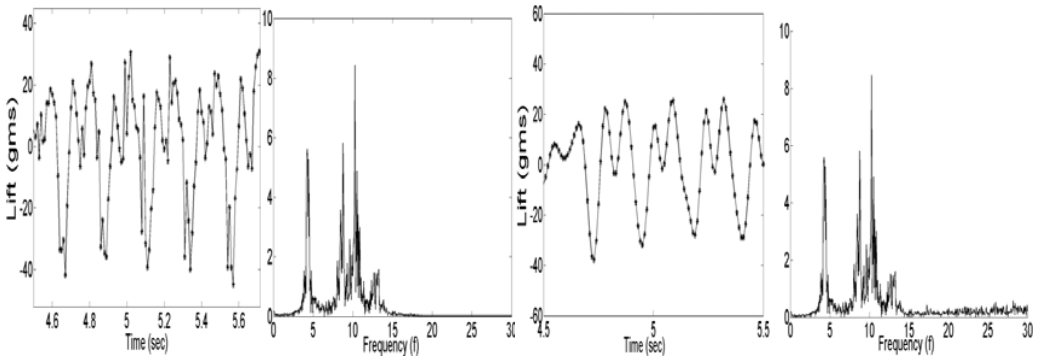

Fig 5.6 (a)raw lift data(b)fft of (a) (c) filtered lift data (d) fft of (c) for 1.75X butterfly wing at Re=4164 at flapping frequency 4.2 Hz on model 3.

In Fig 5.4-5.6, it is shown that given a particular model the kind of flow and nature of forces are same no matter what kind of wing is used. In model 1, whether it is rectangular wing or butterfly wing, the nature of flow (from fft) and the nature of forces with time are same at a particular flapping frequency and same Re range. However due to shape or flexibility the peaks and duration of the latter might shift leading to better averaged forces. From Fig 5.4-5.5 it is clear that the trend of lift on model 1 is similar however due to more sustaining of positive lift in the butterfly wing the average becomes better thus shape factor playing an important role here. In case of Fig 5.6 the model is changed though the butterfly wing is kept the same 1.75X size. But due to change to model 3 and additional feathering and lead lag motion in it the nature of flow and the nature of forces are drastically changed. This shows the inherent dependency on the kinematics of a wing other parameters being same. The effect of flexibility among various rectangular wings have already been discussed earlier.

6. Summary of important findings and conclusions

The total summary and conclusion of this report can be further divided into 3 major sections as per the sequence of experiments.

Flow visualizations:

1. Formation of LEV and its growth has been observed.
2. The effect of stroke reversal from downstroke to upstroke the ejection of the vortex pair has been visualized.
3. The retaining of a part of LEV in the upstroke or wake capture is visualized.

Force experiments:

1. Lift increases predominantly with frequency and Re; it is produced mainly in the downstroke.

2. Thrust increases with frequency as well as with size or the span and is mainly in the stroke reversals for model 1. Thrust is produced in both strokes due to feathering.
3. With forward velocity lift is contributed both from the rotational as well as the translational component (conventional term) of the wing.
4. Model 3 produces more lift and thrust due to its feathering and lead lag motion.
5. Lift and thrust coefficients decrease with increase in advance ratio for both the models (1 and 3)
6. At a particular flapping frequency the coefficients increases with lower Re values for all wings.
7. Rotational component of thrust decreases with increase in frequency for all J values.
8. Rotational component of lift is more or less same for model 1 whereas for model 3 the rotational component of lift increases with frequency reaches a maximum and then decreases again.
9. Lift increases with rigidity and thrust increases with flexibility.
10. Rectangular wing with AR=2 is the optimum wing as it provided the best lift and thrust both.
11. Butterfly wing of 1.75X gives better results compared to rectangular wings owing to its complex shape stabilizing the LEV and delaying its ejection or the diffusion as the case may be.

PIV experiments:

1. LEV and TEV forms as a whole single ring encompassing the whole periphery of the wing.
2. These vortices grow with time and at a particular cross section are opposite and equal in magnitude.
3. The vortices grow till their maximum strength towards the end of downstroke and start diffusing or breaking up.
4. At stroke reversal from downstroke to upstroke other vortex formed below the wing interacts with TEV leading to its ejection. The ejection and its timings are much a parameter depending on the Re number.
5. In the upstroke opposite vortex develops below the wing which grows in size with the progress of this stroke.
6. At the end of the stroke the vortices of both wings interact leading to the clapping effect producing large thrust and lift.
7. The nature of growth of the vortex with the flapping cycle is dependant on Re as well as wing kinematics or the model concerned.
8. The LEV and TEV grows in size circulation and the maximum vorticity contained as shown already, the nature of which depends on the model concerned and the Re involved.
9. The effect of ejection on thrust is shown by performing the momentum analysis and it is seen that the maximum thrust is produced during the stroke reversals either during ejection during clapping if the model allows that.

10. There is a suffcient spanwise flow as noted from the 3D experiments. The ejection is in a direction away from the wing both in the spanwise and chordwise direction.
11. The effect of ejection at the stroke reversals can be seen from the sharp decrease in the circulation curve.
12. The ejection effects are better seen with higher flapping frequency or with higher Re.
13. The vortices are better attached and are intact with model 3. Thus the addition of feathering and lead lag motion cleans the flow making it cleaner.
14. The vorticity of the LEV or TEV increases towards the tip of the wing thus increasing with span. Whereas the size of them depends on the chord length as well which in case of tapered wings decrease along the span. The net effect of both the increased vorticity and size will determine the net strength variation of the LEV making it fall in a particular class which thus depends on the type of wing and on the kinematics as well.
15. In case of model 3 the ejection is not observed due to less flapping velocity or lesser Re involved. Whereas a part of the vortex is retained showing lesser negative lift in the upstroke. This can also be seen through the circulation variation along the cyle.

7. Future Work

As it is evident from so far that the stroke reversals and the wing kinematics during that plays a significant role in the force production, better models can be fabricated that has a play and control in the motion of the wing at these stroke reversals. Hereby more detailed study can be carried out by looking in depth of the dynamics of flow acceleration and vortex growth at this particular time zone. Further beter models can be designed on a miniature level with even more degrees of freedom that can have a better control over the rotational twist at the stroke reversals and the overall lead lag motion followed by the wing tip. Stereoscopic PIV and Time Resolved PIV (TRPIV) experiments will give better insight of the nature of the wake and other unsteady effects present in the flow. The stereoscopic version of TRPIV will be able to show the nature of 3-D wake and flow field and will be able to measure aerodynamic forces with better accuracy. So far all the models being studied have the provision for fixing the wing only by its leading edge to the moving linkage. Later in the future this fixture can be varied to study the effect of the hinge or in general the elastic axis of rotation in the dynamics of flow.Oil tunnel measurement will carried out in near future. At present the tunnel is under construction. Force measurement techniques have to be refined and more sophisticated mechanisms, which will mimic an insect to a greater degree, have to be designed. The wing tip of the insects inscribes an ellipse during a single stroke. The variation of this inscribed ellipse and arrival at an optimum ellipse shape can be studied, as it is indeed an important factor for thrust production. The maneuvering can be studied in details other than the lift and thrust generation once proper model nearly mimicking a particular insect is ready. Force

generations in such unsteady regime is complicated the maneuvering and the control over it will also take sufficient amount of work and effort to be well understood.

References

- Srygley R.B, Thomas A.L.R , 2002, "Unconventional lift generating mechanism in free flying butterflies" *Nature*; **420**, 660-664
- Ellington C.P, Van den Berg C, Willmott A.P, and Thomas A.L.R, 1996 "Leading edge vortices in insect flight" *Nature*; **384**, 626-630
- Dickinson M.H, Lehmann F.O and Sane S.P, 1999 "Wing rotation and the aerodynamic basis of insect flight" *Science*; **284**, 1954-1960
- Philips P.J, East R.A, Pratt N.H, 1981 "An unsteady lifting line theory of flapping wings with application to the forward flight of birds" *Journal of fluid mechanics*; **112**,97-125
- Ellington C.P, 1999 "The Novel Aerodynamics of Insect Flight: Application to Micro Air Vehicles." *J experimental biology*; **202** 3439-48
- Bomphrey R.J, Lawson Nicholas J, Harding Nicholas J, Taylor G.K, Thomas A.L.R, 2004 "The aerodynamics of Manduca sexta: digital Particle Image Velocimetry analysis of the Leading Edge Vortex" *J experimental biology*, **208**, 1079-84
- Sane S.P, 2003, "The aerodynamics of insect flight" *Journal of Experimental Biology* **206**,4191-4208
- Abhijit Banerjee 2005, "Measurement of aerodynamic forces and flow visualization study of butterfly sized elliptic wing flapping models" *IIT kanpur, Mtech Thesis*

List of Publications:

Debopam Das, Saurav K. Ghosh and C. Lakshmana Dora, On Three Dimensional Flow Field of Butterfly Flight, Proceedings of the Indo-US Workshop on Micro Air Vehicles 13-14 November 2008, Bangalore, India

Saurav K. Ghosh, Chandrala L. Dora, Debopam Das, Flow Field of Butterfly Flight: A PIV Study 8TH INTERNATIONAL SYMPOSIUM ON PARTICLE IMAGE VELOCIMETRY - PIV09 Melbourne, Victoria, Australia, August 25-28, 2009

Saurav K. Ghosh, Chandrala L. Dora, Shasant Anand and Debopam Das, Understanding the Role of Unsteady Vortices in Butterfly Flight through PIV Measurements 10th asian symposium of visualization December 7-10, 2009.

Saurav K. Ghosh, Chandrala L dora, GarunendraK Bunkar and Debopam das, Understanding Flapping Flight through PIV Measurements on a Butterfly Simulating Model, ICIUS 2010, 3-5th Nov, 2010

Saurav K. Ghosh, Chandrala L dora, GarunendraK Bunkar and Debopam das, Unsteady Wake characteristics of a flapping wing through 3D TR-PIV, ICIUS 2010, 3-5th Nov, 2010

Manpower: Current: One Sr. Project Mechanic and One Project Associate. One Ph. D. Student (Partially Supported)
Previous: Two Students with M. Tech (For Two months, Partal Support)

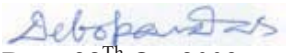

Date: ~~28~~ 28Th ~~Oct 2009~~.

Debopam Das; Ph. D.
Associate Professor
Department of Aerospace Engineering
Indian Institute of Technology Kanpur
Phone: +91 512 259 6163 /7227 /8578
Email: das@iitk.ac.in, debopam_d@yahoo.com